SLAC-PUB-5382
November 1990
(M)

THE INTRINSIC SHORT-DISTANCE STRUCTURE OF HADRONS IN QCD*

STANLEY J. BRODSKY

Stanford Linear Accelerator Center,
Stanford University, Stanford, California 94309, USA

Invited Lectures presented at the 28th International School of Subnuclear Physics:
"Physics up to 200 TeV"
Ettore Majorana Center for Scientific Culture, Erice, Italy, July 16-24, 1990

* Work supported by the Department of Energy, contract DE–AC03–76SF00515.

1. INTRODUCTION

A central problem of particle physics is to determine the composition of hadrons in terms of their fundamental quark and gluon degrees of freedom. The structure of hadronic bound-states in quantum chromodynamics plays a role in virtually every aspect of high energy and weak interaction phenomenology, including jet hadronization, heavy particle production processes at colliders, general exclusive and inclusive reactions, and electro-weak decay matrix-elements. Although the QCD Lagrangian has an elegant simplicity, the structure of its bound state solutions can be extraordinarily rich and complex. In these lectures I will focus on QCD phenomena which reflect the coherence and composition of hadron wave functions as relativistic many-body systems of quark and gluon quanta.[1]

There are many different ways in which experiment can resolve the short-distance structure of hadrons. It is necessary to distinguish "intrinsic" versus "extrinsic" contributions to scattering reactions. The intrinsic contributions, which are associated with multiparticle interactions within the hadronic bound state, have lifetimes much longer than that of the time of collision; they are thus formed before the collision and lead to process-independent Feynman scaling production cross sections. Extrinsic contributions, on the other hand, are controlled by the high momentum transfer scale of the collision process itself and have short lifetimes of the same order as that of the collision time. Extrinsic contributions provide the leading twist radiative corrections associated with the renormalization of single quark or gluon lines and the QCD evolution of structure functions.

Data from many sources suggest that the intrinsic bound state structure of the nucleon has a non-negligible strange- and charm-quark content in addition to the extrinsic sources of heavy quarks created in the collision itself. In fact, QCD predicts that the hadronic wave-function has an "intrinsic hardness,"[2] which leads to a non-negligible probability for high mass and high momentum short-range fluctuations. In fact, because of asymptotic freedom, one can analyze short-distance, high momentum transfer, and heavy quark fluctuations of a hadronic wave function perturbatively. The probability that a hadronic wave functions has far-off-shell fluctuations is only power-law suppressed in QCD because of the point-like character of the quark-gluon interactions. For example, the probability that a heavy quark pair exists virtually in a light hadron only decreases as $P_{Q\overline{Q}} \sim \alpha_s^2(M_Q^2)/M_Q^2$. This key property of the theory has a number of important implications for the production of heavy quark and other massive systems with large momentum fractions x in inclusive reactions and also in exclusive reactions at threshold. The intrinsic fluctuations have a Lorentz-boosted virtual lifetime of order $\tau \propto \gamma/M_Q^2$. Thus they can be materialized in high energy collisions as projectile fragments. The dependence of the hidden and open heavy quark production cross sections on the size of a nuclear target can be used as a filter to identify these intrinsic heavy quark processes. Further discussion will be given in Sections 2 and 5.

An important tool for analyzing the underlying structure of a complex system is to change its external conditions. In the case of quantum electrodynamics, one can use external Stark and Zeeman fields to perturb atomic wave functions and probe their composite structure. Analogously, in QCD, we can use a nuclear medium to modify and probe short-distance hadronic structure and dynamics. In fact, as I discuss in Section 2, we can use the nucleus as a differential "color filter"[3,4] to separate Fock components (or fluctuations) of different transverse size in the projectile's wave function and to separate perturbative short-distance subprocesses from non-perturbative mechanisms. I also will discuss "color transparency"[5] as a way to isolate strictly perturbative contributions to large angle exclusive scattering In this analysis' we will see how strong binding effects at the charm threshold complicates perturbative QCD predictions, explaining both the anomalous spin correlation A_{NN} observed in large angle pp scattering at $\sqrt{s}$ and the anomalous decrease of color transparency seen in quasi-elastic pp scattering in nuclei at the same energy. The strong interactions of colored particles at small relative velocity also leads to other interesting phenomena, including the production of nuclear-bound charmonium near threshold and the suppression of *J/psi* production coalescence of charm quarks with co-moving spectators.' I also will discuss in Section 6 a new approach' to shadowing and anti-shadowing of nuclear structure functions, and how these phenomena can provide information on the phase and magnitude of quark or gluon scattering amplitudes in the nuclear medium.

In Section 3 I will present some new results for the intrinsic polarized and unpolarized gluon distributions of the proton which are associated with hadron binding.' These discussions are important in regard to understanding the EMC spin crisis problem.[10] It is also important to note that the conventionally-defined "valence" distributions measured in deep inelastic lepton scattering are actually not identical to the bound state valence quark distributions because of a subtle effect due to Pauli blocking.? This is discussed in detail in Section 4.

The above ingredients provide the foundations for analyzing many novel features of hadronic and heavy quark processes in high energy collisions including color transparency and intrinsic charm reactions.

1.1. Relativistic Wavefunctions in Gauge Theory

How can one define a wave function of a composite system in a relativistic quantum gauge field theory? A natural description, similar physically to that of the parton model, is to utilize a Fock expansion at fixed time $\tau = t - z/c$ on the light cone. This description is particularly simple since the perturbative vacuum is an apparent eigenstate of the full theory. As discussed recently by Werner,[12] the rigorous quantization of gauge theories on the light cone allows zero mode degrees of freedom of the gauge field in the vacuum sector which corresponds to non-zero chiral charge and other topological vacuum properties. In the particle sector of the theory, where one can quantize the theory in the light cone gauge $A^+ = 0$, one obtains a Fock basis containing only physical degrees of freedom.

The hadron eigenstate state can thus be expanded on the complete set of free quark and gluon eigenstates of the free QCD Hamiltonian which have the same global quantum numbers as the hadron: e.g.:

$$\begin{aligned} |\Psi_p\rangle = \sum |n\rangle \langle n \,|\, \Psi_p\rangle \\ = \quad & |uud\rangle \, \psi_{uud}(x_i, k_{\perp i}, \lambda_i) \\ & + |uudg\rangle \, \psi_{uudg}(x_i, k_{\perp i}, \lambda_i) \\ & + |uudq\bar{q}\rangle \, \psi_{uudq\bar{q}}(x_i, k_{\perp i}, \lambda_i) \\ & + \dots \end{aligned} \tag{1}$$

The x_i are the light-cone momentum fractions $x_i = (k^0 + k^z)/(P^0 + P^z)$, with $\sum_{i=1}^{n} x_i = 1$, and $\sum k_{\perp i} = 0$. The wave functions $\psi_n(x_1, k_{\perp i}, \lambda_i)$ appearing in the Fock-state expansion contain the physics of the hadron entering scattering amplitudes. For example, the structure functions measured in deep inelastic scattering are constructed as probability distributions in x from the sum of the squares of the light-cone wave functions $\psi_n(x_i, k_{\perp i}, \lambda_i)$. (See Section 4.) Similarly, since the current is a simple diagonal local operator on the free quark basis, form factors can be computed from a simple overlap integral of the ψ_n. More generally, high momentum transfer exclusive reactions in QCD are sensitive to each hadron's distribution amplitude $\phi(x_i, Q)$, which is the valence Fock amplitude integrated over transverse momentum up to the scale Q.

The problem of solving QCD, including its bound state color-singlet spectrum and wavefunctions, is equivalent to the diagonalization of the QCD Hamiltonian. A frame-invariant Hamiltonian operator can be obtained by quantizing the theory at fixed light-cone time. This is the "light-front" formulation of Hamiltonian theory described by Dirac which produces the maximal number of interaction-free commuting invariants including the total light-cone momentum P^+ and transverse momentum $P_\perp$. The τ evolution operator $P^- = P^0 - P^z$ may be written in the general form $P^- = (H_{LC} + P_\perp^2)/P^+$ so that the eigenvalues of the operator H_{LC}

are exactly the squares of invariant masses of the spectrum. The eigenvalue problem is thus $H_{LC}|\Psi>= \mathcal{M}^2|\Psi>$. It should be emphasized that the light-cone Hamiltonian is completely independent of the total momentum of the system P^+ and $P_\perp$ and is a Lorentz scalar. If we choose the light-cone Fock representation described above, then we obtain a covariant Heisenberg matrix representation of the theory: $< n|H_{LC}|m >< m|\Psi >= \mathcal{M}^2|\Psi.>$ The projections of the eigenfunctions on this basis are precisely the wavefunctions needed for phenomenology. The QCD Hamiltonian can be elegantly quantized on the light-cone in $A^+ = 0$ gauge without resort to unphysical ghost quanta, even in non-Abelian gauge theory.'

1.2. Discretized Light-Cone Quantization

In order to make the eigenvalue problem tractable for numerical analysis, it is convenient to choose a discrete momentum Fock basis. In the method of Discretized Light-Cone Quantization,[13] one constructs a discrete basis of discrete momentum–space color-singlet free gluon and quark light-cone Fock states satisfying periodic and anti-periodic boundary conditions, respectively. Again the analysis is frame independent. The matrix elements of the QCD Hamiltonian are extremely simple in this basis. Because of momentum and flavor conservation laws obeyed by the interaction Hamiltonian, the matrix is sparse far from the diagonal. A covariant truncation to a finite system is obtained by choosing a global, gauge invariant cut-off on the maximum invariant mass of the Fock state. A local cut-off on the change of mass across the matrix element can serve as an ultraviolet cut-off. In each case, the regulators refer to the continuum theory. The discretization is not used to regularize the theory. In DLCQ one can either numerically diagonalize the light-cone Hamiltonian on the Fock basis, or project the eigenvalue problem onto the lowest number (valence) Fock component and then numerically solve the resulting integral equation. The DLCQ formalism is defined such that each step, including ultraviolet regularization and Fock space truncation, is Lorentz-frame independent. The computer program only involves relative coordinates and is independent of the total momentum $(P^+, P_\perp.)$ The discrete formulation thus provides a finite, Lorentz invariant, and faithfully renormalizable representation of the full quantum field theory in the physical particle sector. IN DLCQ the discretization can be kept independent of the ultraviolet regulators which are set by the continuum theory. Again, unlike lattice gauge theory, there are no special difficulties with fermions.

In principle, the eigenvalues obtained by diagonalizing of the light-cone Hamiltonian in the DLCQ basis provide the entire invariant mass spectrum and eigenfunctions needed to compute the hadron matrix elements,form factors, and the structure functions and distribution amplitudes entering QCD factorization formulae. A major success of DLCQ has been its applications to gauge theories in one-space and one-time dimensions.[14] For example, the complete spectrum and the respective structure functions of mesons, baryons, and nuclei in QCD($1+1$) for $SU(3)_C$ have been obtained as a function of mass and coupling constant. Results for the structure function of the lowest mass meson and baryon at weak and strong coupling are shown in Fig. 1.

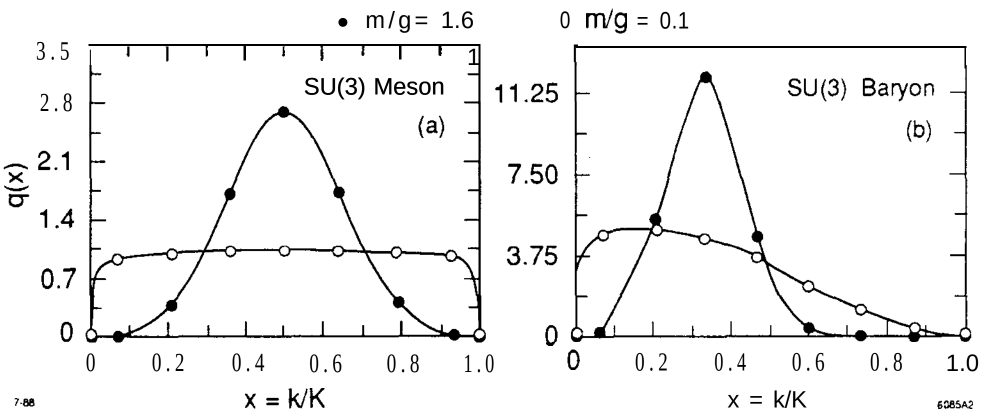

Figure 1. Valence structure functions of the baryon and meson in QCD in one–space and one–time dimension. The results are for one quark flavor and three colors.

The application of DLCQ to gauge theory in three-space and one-time dimensions is a much more challenging computational task, but significant progress has recently been made computing the fine structure and hyperfine spectrum of positronium in strong coupled QED.[15]

Important constraints and information on the non-perturbative structure of the proton in QCD models have also been obtained using bag models, quark–diquark schemes, QCD sum rules, non-relativistic quark models, and lattice gauge theory. A summary and references may be found in Ref. 1.

2. THE NUCLEUS AS A QCD FILTER

There are many important ways in which a nuclear target can probe fundamental aspects of QCD. A primary concept is that of the "color filter":[3,4] if the interactions of an incident hadron are controlled by gluon exchange, then the nucleus will be transparent to those fluctuations of the incident hadron wave function which have small transverse size. Such Fock components have a small color dipole moment and thus will interact weakly in the nucleus; conversely, Fock components of normal hadronic size will interact strongly and be absorbed during their passage through the nucleus: For example, large momentum transfer quasi-exclusive reactions,[16] are controlled in perturbative QCD by small color-singlet valence-quark Fock components of transverse size $b_\perp \sim 1/Q$; thus initial-state and final-state corrections to these hard reactions are suppressed at large momentum transfer, and they can occur in a nucleus without initial or final state absorption or multiple scattering of the interacting hadrons. Thus, at large momentum transfer and energies, quasi-elastic exclusive reactions are predicted to occur uniformly in the nuclear volume. This remarkable phenomenon is called "color transparency."[5] Thus QCD predicts that the transparency ratio of quasi-elastic annihilation of the anti-proton in the $\overline{p}p \to \ell\overline{\ell}$ reaction will be additive in proton number in a nuclear target:[17, 18]

$$\frac{\frac{d\sigma}{dQ^2}(\overline{p}A \to \ell\overline{\ell}(A-1))}{\frac{d\sigma}{dQ^2}(p\overline{p} \to \ell\overline{\ell})} \to Z^1 \tag{2}$$

for large pair-mass squared Q^2. In contrast to the QCD color transparency prediction, the traditional (Glauber) theory of nuclear absorption predicts that quasi–elastic scattering occurs primarily on the front surface of the nucleus. The above ratio thus should be proportional to $Z^{2/3}$, i.e. the number of protons exposed on the nuclear surface.

Conditions for Color Transparency — Color transparency is a striking prediction of perturbative QCD at high momentum transfers. There are two conditions which set the kinematic scale where the effect should be evident. First, the hard scattering subprocess must occur at a sufficiently large momentum transfer so that only small transverse size wave function components $\psi(x_i, b_\perp \sim 1/Q)$ with small color dipole moments dominate the reaction. Second, the state must remain small during its transit through the nucleus. The expansion distance is controlled by the time in which the small Fock component mixes with other Fock components. By Lorentz invariance, the time scale $\tau = 2E_{\overline{p}}/\Delta\mathcal{M}^2$ grows linearly with the energy of the hadron in the nuclear rest frame, where $\Delta\mathcal{M}^2$ is the difference of invariant mass squared of the Fock components. Estimates for the expansion time are given in Refs. 4, 19, and 20.

There are a number of important tests of color transparency and color filter that can be carried out with anti-proton beams of moderate energy.[21] Since total annihilation processes such as $p\overline{p} \rightarrow \ell\overline{\ell}$ or $p\overline{p} \rightarrow \gamma\gamma$ and $p\overline{p} \rightarrow J/\psi$ automatically involve short distances, the first condition for color transparency should be satisfied. The study of the energy dependence of these processes inside nuclei (quasi-elastic reactions, integrated over Fermi-motion) can clarify the role of the expansion time scale τ. A recent analysis by Jennings and Miller" shows that $\tau = 2E_{\overline{p}}/\Delta\mathcal{M}^2$ is controlled by the mass difference of states which are close in mass to that of the asymptotic hadronic state. Thus color transparency may well be visible in low energy anti-proton annihilation processes, including quasi-elastic $\overline{p}p \rightarrow J/\psi$ and $\overline{p}p \rightarrow \overline{\ell}\ell$ annihilation in the nucleus.

The only existing test of color transparency is the measurement of quasi-elastic large angle pp scattering in nuclei at Brookhaven.[18] The transparency ratio is observed to increase as the momentum transfer increases, in agreement with the color transparency prediction. However, in contradiction to perturbative QCD expectations, the data suggests, surprisingly, that normal Glauber absorption seems to recur at the highest energies of the experiment $p_{\rm lab} \sim 12\ GeV/c$. It should be noted that this is the same kinematic domain where a strong spin correlation A_{NN} is observed.[22] The probability of protons scattering with their spins parallel and normal to the scattering plane is found to be **four times** that of anti-parallel scattering, which is again in strong contradiction to QCD expectations. However, Guy De Teramond and I[6] have noted that the breakdown of color transparency and the onset of strong spin-spin correlations can both be explained by the fact that the charm threshold occurs in pp collisions at $\sqrt{s} \sim 5\ GeV$ or $p_{\rm lab} \sim 12\ GeV/c$. At this energy the charm quarks are produced at rest in the center of mass. Since all of the eight quarks have zero relative velocity, they can resonate to give a strong threshold effect in the $J = L = S = 1$ partial wave. (The orbital angular momentum of the pp state must be odd since the charm and anti-charm quarks have opposite parity.) This partial wave predicts maximal spin correlation in A_{NN}. Most important, such a threshold or resonant effect couples to hadrons of conventional size which will have normal absorption in the nucleus. If this non-perturbative $pp \rightarrow pp$ amplitude dominates over the perturbative QCD amplitude, one can explain both the large spin correlation and the breakdown of color transparency at the charm threshold. Thus the nucleus acts as a filter, absorbing the non-perturbative contribution to elastic pp scattering, while allowing the hard scattering perturbative QCD processes to occur additively throughout the nuclear volume.[23] Similarly, one expects that the charm threshold will modify the color transparency and hard-scattering behavior of quasi-elastic $\overline{p}p$ reactions in nuclei at energies $\sqrt{s} \sim 3\ GeV$.

Diffractive Production of Jets in Anti-Proton Nuclear Reactions — In our original paper on the color filter, Bertsch, Goldhaber, Gunion, and I[3] suggested that diffractive nuclear reactions could be used as a color filter, i.e. fluctuations of an incident hadron with small color dipole moments and hence could emerge unscathed after transit through a nucleus without nuclear excitation. In the case of anti-proton reactions, the fluctuations of the valence Fock state where the three anti-quarks has small transverse separation and thus small color dipole moment will be produced in the form of three jets on the back side of the nucleus. The longitudinal and transverse momentum dependence of the $\overline{p}A \to A\ Jet\ Jet\ Jet$ cross section will reflect the $\overline{qqq}$ composition of the incident anti-proton wave function.

The Color Filter and Hadron Fragmentation in Nuclei — Recently, Hoyer and I[24] have shown that the color filter ansatz can explain the empirical rule that the nuclear dependence of hadronic spectra $\frac{d\sigma/dx_F(HA\to H'X)}{d\sigma/dx_F(HN\to H'X)} = A^{\alpha(x_F)}$, is nearly independent of particle type *H'*. The essential point is that fluctuations of the initial hadron *H* which have the small transverse size have the least differential energy loss in the nucleus.

Color Transparency and Intrinsic Charm — A remarkable feature of the hadronic production of the J/ψ by protons in nuclei[25,26] is the fact that the cross section persists to high x_F, but with a strongly suppressed nuclear dependence, $A^{\alpha(x_F)} \sim 0.7$. The magnitude of the cross sections for high momentum charmonium reported by the NA-3 group[25] at CERN is, in fact, far in excess of what is predicted from gluon fusion or quark anti-quark annihilation subprocesses. Both the anomalous A-dependence and the high–x_F excess can be explained by assuming the presence of intrinsic charm components of the incident hadron wave–functions.[24] The essential physics point is as follows: the intrinsic charm Fock components, e.g. $|uudc\overline{c}\rangle$ in the proton have maximum probability when all of the quarks have equal velocities, *i.e.* when $x_i \propto \sqrt{m^2 + k_{\perp_i}^2}$. This implies that the charm and anti-charm quarks have the majority of the momentum of the proton when they are present in the hadron wave function. In a high energy proton–nucleus collision, the small transverse size, high-x intrinsic $c\overline{c}$ system can penetrate the nucleus, with minimal absorption and can coalesce to produce a charmonium state at large x_F. The remaining spectators of the nucleon tend to have more normal transverse size and interact on the front surface of the nucleus, leading to a production cross section approximately proportional to $A^{0.7}$. Since the formation of the charmonium state occurs far outside the nucleus at high energies, one predicts similar $A^{\alpha(x_F)}$–dependence of the J/ψ and ψ' cross sections, in agreement with recent results reported by the E-772 experiment at Fermilab.[26] Further discussion on the implications of intrinsic charm is given in Section 5.

Shadowing, Anti-Shadowing of Inclusive Anti-Proton Reactions — In the case of inclusive reactions, such as Drell-Yan massive lepton pair production $p\overline{p} \to \ell\bar{\ell}X$, multiple scattering of the interacting partons in the nucleus can lead to shadowing and anti-shadowing of the nuclear structure functions and a shift of the pair's transverse momentum to large transverse momentum. Hung Jung Lu and I have shown that nuclear shadowing of leading-twist QCD reactions can be related to Pomeron exchange in the multiple interactions of the quark or anti-quark in the nucleus, and that the complex phase of the quark-nucleon scattering amplitude due to non-singlet Reggeon exchange leads to anti-shadowing; i.e. an excess of the nuclear cross section over nucleon additivity.[8] A detailed discussion will be given in Section 6.

Formation Zone Effects in Inclusive Reactions — An essential aspect of the proofs of QCD factorization of inclusive reactions such as Drell-Yan massive lepton pair production in a nuclear target is that the entire nuclear dependence of the cross section is contained in the nuclear structure functions as measured in deep inelastic lepton-nucleus scattering. Thus the factorization theorem predicts that there is no initial state absorption or scattering that can significantly modify an incident hadron's parton distributions as it propagates through the nucleus. In particular, induced hard colinear radiation due to inelastic reactions in the nucleus before the annihilation or hard-scattering subprocess occurs must be dynamically suppressed. As shown by Bodwin, Lepage, and myself:' this suppression occurs automatically in the nucleus due to the destructive interference of the various multiple-scattering reactions in the nucleus. The interference occurs if the inelastic processes can occur coherently in the nucleus. This requires that the momentum transfer to target nucleons must be small compared to the inverse correlation length in the nucleus; *i.e.* $E_{\overline{q}} > \Delta\mathcal{M}^2 L_A > 1$, where E_q is the laboratory energy of the annihilating anti–quark, $\Delta\mathcal{M}^2$ is the change of mass squared of the quark in the inelastic reaction (small for hard colinear gluon emission of the anti-quark), and L_A is the length between target centers in the nucleus. This formation zone effect can be studied in detail by measuring the nuclear dependence as a function of anti-quark laboratory energy in anti-proton reactions.

Exclusive Nuclear Amplitudes — Exclusive nuclear reactions such as $\overline{p}d \to \gamma n$ or $\overline{p}d \to \pi^0 n$ can provide an important test of the reduced amplitude formalism for large momentum transfer exclusive nuclear reactions. Recent measurements at SLAC[28] are in striking agreement with the reduced amplitude predictions for photo-disintegration $\gamma d \to np$ at a surprising low momentum transfer. The corresponding anti-proton reactions will allow an important test of both the scaling behavior of exclusive nuclear reactions and their crossing behavior to the annihilation channel.

Hidden Color Nuclear Components — In QCD the six-quark deuteron is a linear superposition of five color singlet states, only one of which corresponds to the conventional $n-p$ state.[29] One can search for hidden color excitations of the deuteron in $\overline{p}He^3$ elastic scattering at large angles.

Nuclear Bound Quarkonium — The production of charmonium at threshold in a nuclear target is particularly interesting since it is possible that the attractive QCD van der Waals potential due to multi-gluon exchange could actually bind the η_c to light nuclei. Consider the reaction $\overline{p}\alpha \rightarrow (c\overline{c})H^3$ where the charmonium state is produced nearly at rest. (See Fig. 2.) At the threshold for charm production, the incident nuclei will be nearly stopped (in the center of mass frame) and will fuse into a compound nucleus because of the strong attractive nuclear force. The charmonium state will be attracted to the nucleus by the QCD gluonic van der Waals force. One thus expects strong final state interactions near threshold. In fact, Guy De Teramond, Ivan Schmidt, and I[30] have argued that the $c\overline{c}$ system will bind to the H^3 nucleus. It is thus likely that a new type of exotic nuclear bound state will be formed: charmonium bound to nuclear matter. Such a state should be observable at a distinct $\overline{p}\alpha$ center of mass energy, spread by the width of the charmonium state, and it will decay to unique signatures such as $\overline{p}\alpha \rightarrow H^3\gamma\gamma$. The binding energy in the nucleus gives a measure of the charmonium's interactions with ordinary hadrons and nuclei; its hadronic decays will measure hadron-nucleus interactions and test color transparency starting from a unique initial state condition.

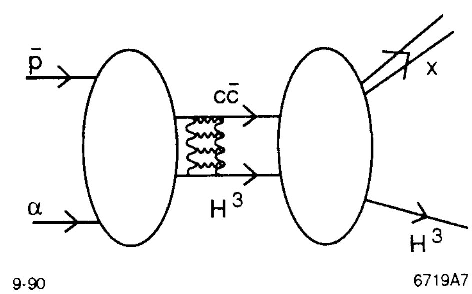

Figure 2. Formation of the $(c\overline{c})-H^3$ bound state in the process $\overline{p}\alpha \rightarrow H^3X$.

In QCD, the nuclear forces are identified with the residual strong color interactions due to quark interchange and multiple-gluon exchange. Because of the identity of the quark constituents of nucleons, a short-range repulsive component is also present (Pauli-blocking). From this perspective, the study of heavy quarkonium interactions in nuclear matter is particularly interesting: due to the distinct flavors of the quarks involved in the quarkonium-nucleon interaction there is no quark exchange to first order in elastic processes, and thus no one-meson-exchange potential from which to build a standard nuclear potential. For the same reason, there is no Pauli-blocking and consequently no short-range nuclear repulsion. The nuclear interaction in this case is purely gluonic and thus of a different nature from the usual nuclear forces.

The production of nuclear-bound quarkonium would be the first realization of hadronic nuclei with exotic components bound by a purely gluonic potential. Furthermore, the charmonium-nucleon interaction would provide the dynamical basis for understanding the spin-spin correlation anomaly in high energy $p-p$ elastic scattering: In this case, the interaction is not strong enough to produce a bound state, but it can provide a strong enough enhancement at the heavy-quark threshold characteristic of an almost-bound system?

3. INTRINSIC GLUON DISTRIBUTIONS

The *intrinsic* gluon distribution $G_{g/H}(x, Q_0^2)$ describes the fractional light-cone momentum distribution of gluons associated with the bound-state dynamics of the hadron H, in distinction to the *extrinsic* distribution, which is derived from radiative processes or evolution. Given the intrinsic distribution, one can obtain the extrinsic distribution by applying the QCD evolution equations starting at the bound-state scale Q_0.

In principle, one must solve the non-perturbative bound state equation of motion to compute the intrinsic gluon distribution. In the case of positronium in quantum electrodynamics one can readily calculate the photon distribution, at least to first order in the fine structure constant α. The analysis requires coherence between amplitudes in which the electron and positron couple to the photons. In the infrared limit this coherence in the neutral atom ensures a finite photon distribution.

In the QCD case, the analysis of the intrinsic gluon distribution of a hadron is essentially non-perturbative. However, there are several theoretical constraints which limit its form:

1. In order to insure positivity of fragmentation functions, distribution functions $G_{a/b}(x)$ must behave as an odd or even power of $(1-x)$ at $x \rightarrow 1$ according to the relative statistics of a and b.[32] Thus the gluon distribution of a nucleon must have the behavior: $G_{g/N}(x) \sim (1-x)^{2k}$ at $x \rightarrow 1$ to ensure correct crossing to the fragmentation function $D_{N/g}(z)$. This result holds individually for each helicity of the gluon and the nucleon.
2. The coupling of quarks to, gluons tends to match the sign of the quark helicity

to the gluon helicity in the large x limit.[33] We define the helicity-aligned and anti-aligned gluon distributions: $G^+(x) = G_{g\uparrow/N\uparrow}(x)$ and $G^-(x) = G_{g\downarrow/N\uparrow}(x)$. The gauge theory couplings imply

$$\lim_{x \to 1} G^-(x)/G^+(x) \to (1-x)^2. \tag{3}$$

3. In the low x domain the quarks in the hadron radiate gluons coherently, and one must compute emission of gluons from the quark lines taking into account interference between amplitudes. We define $\Delta G(x) = G^+(x) - G^-(x)$ and $G(x) = G^+(x) + G^-(x)$. We shall show that the asymmetry ratio $\Delta G(x)/G(x)$ vanishes linearly with x; perhaps coincidentally, this is also the prediction from Reggeon exchange:' The coefficient at $x \to 0$ depends on the hadronic wave functions; however, for equal partition of the hadron's momentum among its constituents, we will show that

$$\lim_{x \to 0} \Delta G(x)/G(x) \to N_q\, x, \tag{4}$$

where N_q is the number of valence quarks.

4. In the $x \to 1$ limit, the stuck quark is far off-shell so that one can use perturbation theory to characterize the threshold dependence of the structure functions. We find for three-quark bound states

$$\lim_{x \to 1} G^+(x) \to C(1-x)^{2N_q-2} = C(1-x)^4, \tag{5}$$

Thus $G^-(x) \to C(1-x)^6$ at $x \sim 1$. This is equivalent to the spectator–counting rule developed in Ref. 35.

Ivan Schmidt and I" have proposed a simple analytic model for the intrinsic gluon distribution in the nucleon which incorporates all of the above constraints:

$$\Delta G(x) = \frac{N}{x}[5(1-x)^4 - 4(1-x)^5 - (1-x)^6] \tag{6}$$

and

$$G(x) = \frac{N}{x}[5(1-x)^4 - 4(1-x)^5 + (1-x)^6] \tag{7}$$

In this model the momentum fraction carried by intrinsic gluons in the nucleon is $< x_g >= \int_0^1 dx x G(x) = (10/21)N$, and the helicity carried by the intrinsic gluons is $\Delta G \equiv \int_0^1 dx \Delta G(x) = 7/6N$. The ratio $\Delta G/ < x_g >= 49/20$ for the intrinsic gluon distribution is independent of the normalization N. Phenomenological analyses imply that the gluons carry approximately one-half of the proton's momentum: $< x_{g/N} > \simeq 0.5$. We shall assume that this is a good characterization of the intrinsic gluon distribution. The momentum sum rule then implies N $\sim$ 1 and AG $\sim$ 1.2. A review of the present experimental and theoretical limits on gluon and quark spin in the nucleon is given in Ref. 10.

In the following sections I will discuss an analysis by Schmidt and myself[9] of both the polarized and unpolarized intrinsic gluon distribution functions. First we study the behavior of the gluon asymmetry (unpolarized over polarized distributions) in the small x region where it turns out to be approximately independent on-the details of the bound-state wave function. The logarithmic ultra-violet cut-off dependence of the intrinsic distribution matches with the lower cut-off of the extrinsic distribution; the Q^2 evolution of the extrinsic distribution is studied in detail in Ref. 36.

In Section 3 we shall show that the intrinsic gluon distribution is related to the retarded part of the spin-dependent bound-state potential $-\left\langle \frac{\Delta \partial V}{\partial M_B^2} \right\rangle_{hfs}$. This allows us to derive sum rules for the difference of gluon distribution (and fragmentation) functions for hadrons with different spin in terms of the spin-dependent part of the bound-state potential.

3.1. Intrinsic Gauge Field Distributions

A general bound-state wave function can be expanded in terms of (Fock) states of definite number (n) of elementary free fields. We define the Fock expansion at equal "time" $\tau = t + z$ in the light cone gauge $A^+ = A^0 + A^3 = 0$. Labelling the corresponding renormalized amplitudes as $\psi^{(Q)}_{n/B}(x_i, \vec{k}_{\perp_i}, \lambda_i)$, the distribution function for a constituent $\underline{a}$ in the bound state $\underline{B}$ (see Ref. 37 for details and definitions) is given by:

$$G_{a/B}(x, Q^2) = \sum_{n,\lambda_i} \int \overline{\prod_{i}} \frac{dx_i d^2 k_{\perp_i}}{16\pi^3} |\psi^{(Q)}_{n/B}(\psi_i, \vec{k}_{\perp_i}, \lambda_i)|^2 \sum_b \delta(x_b - x) \quad . \quad (8)$$

We first consider positronium as an example, and calculate the intrinsic distribution function of photons $G_{\gamma/positronium}$. To leading order in the binding energy we can neglect pair annihilation, pair production, and higher particle number Fock states.

The distribution function for positive helicity photons G^+ is calculated from the diagrams of Fig. 3(a) for the case of J_z = \$1 ortho-positronium $(u_\uparrow \overline{v}_\uparrow)$. Similarly, the corresponding diagrams for negative helicity photons are shown in Fig. 3(b), where an arrow up $\uparrow$ (down $\downarrow$) indicates positive (negative) helicity. In the diagrams, the upper fermion line corresponds to a particle (electron), and the lower to

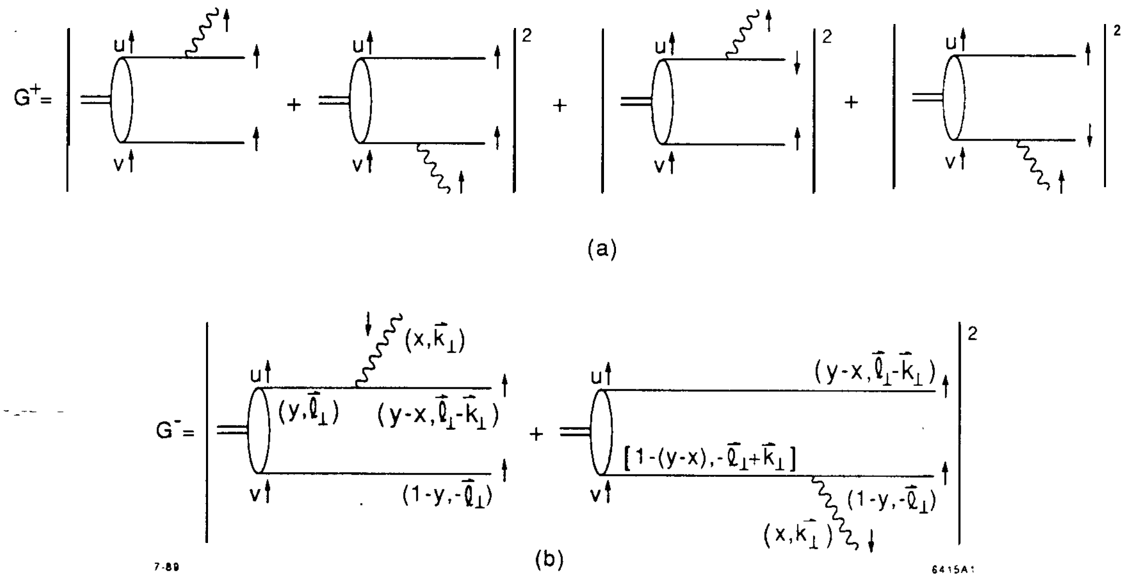

Figure 3. Diagrams that contribute to the distribution function for positive polarized photons (a), and for negative polarized photons (b), for $J_z = +1$ ortho–positronium $(u_\uparrow \bar{v}_\uparrow)$.

an antiparticle (positron). We have also indicated the light-cone parameterization of momenta that we will use when the photon couples to an electron or positron. With this choice, the photon is always parameterized by $(x, \vec{k}_\perp)$ and the final state has the same form in all cases. The appropriate matrix elements for the various helicity transitions are given in Ref. 38.

The calculation is now straightforward. If we denote by $\psi(y, \vec{\ell}_\perp)$ the two-body bound-state valence wave function (lowest Fock state amplitude), the results are:

$$
\begin{aligned}
G^{+}_{\gamma/\mathrm{ortho}\uparrow}(x,\vec{k}_\perp) &= \frac{\alpha}{2\pi^2}\int \frac{d^2\ell_\perp}{2(2\pi)^3}\int_x^1 dy \\
&\times \Bigg\{ \left[\psi(y,\vec{\ell}_\perp)\,\frac{y\vec{k}_\perp - x\vec{\ell}_\perp}{y-x} - \psi(y-x,\,\vec{\ell}_\perp-\vec{k}_\perp)\,\frac{(1-y)\,\vec{k}_\perp + x\,\vec{\ell}_\perp}{1-y} \right]^2 \frac{1}{x^3} \\
&+ \Bigg[\left|\,\psi(y,\vec{\ell}_\perp)\,\right|^2 \frac{1}{(y-x)^2 y^2} \\
&+ \left|\,\psi(y-x,\vec{\ell}_\perp-\vec{k}_\perp)\,\right|^2 \frac{1}{(1-y)^2\,(1-[y-x])^2} \Bigg]\; x\,m^2 \Bigg\}\, \frac{1}{D^2}\,,
\end{aligned}
\tag{9}
$$

$$G^{-}_{\gamma/\mathrm{ortho}\uparrow}(x,\vec{k}_\perp) = \frac{\alpha}{2\pi^2}\int\frac{d^2\ell_\perp}{2(2\pi)^3}\int\limits_x^1 dy$$

$$\times\left[\psi(y,\vec{\ell}_\perp)\,\frac{y\vec{k}_\perp - x\vec{\ell}_\perp}{y} - \psi(y-x,\,\vec{\ell}_\perp-\vec{k}_\perp)\,\frac{(1-y)\,\vec{k}_\perp + x\,\vec{\ell}_\perp}{1-(y-x)}\right]^2\frac{1}{x^3D^2},$$

where

$$D = M_B^2 - \frac{(\vec{\ell}_\perp-\vec{k}_\perp)^2+m^2}{y-x} - \frac{\vec{\ell}_\perp^2+m^2}{1-y} - \frac{\vec{k}_\perp^2}{x}. \tag{10}$$

Here m and M_B are the electron and bound state masses, respectively. The intrinsic gluon distribution defined in Eq. (8) is obtained by integrating these expressions over the transverse momentum up to the cut-off Q_0^2. The same approach gives

$$G^{+}_{\gamma/\mathrm{para}} = G^{-}_{\gamma/\mathrm{para}}, \tag{11}$$

$$G^{+}_{\gamma/\mathrm{ortho}\;J_z=0} = G^{-}_{\gamma/\mathrm{ortho}\;J_z=0}.$$

The polarized and unpolarized photon distribution functions are given by:

$$\begin{aligned}\Delta G(x,\,\vec{k}_\perp) &\equiv G^{+}(x,\,\vec{k}_\perp) - G^{-}(x,\,\vec{k}_\perp),\\ G(x,\,\vec{k}_\perp) &\equiv G^{+}(x,\,\vec{k}_\perp) + G^{-}(x,\,\vec{k}_\perp).\end{aligned} \tag{12}$$

Let us now consider the small x limit for these functions. Expanding around x = 0, we readily obtain:

$$\Delta G(x\sim 0,\vec{k}_\perp) = \frac{\alpha}{\pi^2\vec{k}_\perp^2}\int\frac{d^2\ell_\perp}{2(2\pi)^3}\int\limits_0^1 dy\left[\psi(y,\vec{\ell}_\perp) - \psi(y,\vec{\ell}_\perp-\vec{k}_\perp)\right]$$

$$\times\left[\frac{\psi(y,\vec{\ell}_\perp)}{y} - \frac{\psi(y,\vec{\ell}_\perp-\vec{k}_\perp)}{1-y}\right] \tag{13}$$

and

$$G(x\sim 0,\,\vec{k}_\perp) = \frac{\alpha}{\pi^2\vec{k}_\perp^2 x}\int\frac{d^2\ell_\perp}{2(2\pi)^3}\int\limits_0^1 dy\left[\psi(y,\vec{\ell}_\perp) - \psi(y,\vec{\ell}_\perp-\vec{k}_\perp)\right]^2.$$

The infrared singularity at $\vec{k}_\perp^2 \to 0$ is eliminated because of the neutrality of the atom.

It should be noted that the singularity in $G(x, \vec{k}_\perp)$ at x $\to$ 0 is actually an ultraviolet singularity for any non-zero value of $\vec{k}_\perp$ since x = $(k^0 + k^z)/(p^0 + p^z)$ can only be zero if $k_z \to$ -co. By definition, the intrinsic distribution $G(x, Q_0^2)$ refers to Fock states with limited parton invariant mass *M:* $\mathcal{M}^2 = \sum_i \left[\frac{\vec{k}_\perp^2 + m^2}{x} \right]_i < Q_0^2$. This restriction regularizes the x $\to$ 0, $\vec{k}_\perp \neq 0$ region. On the other hand, the extrinsic contribution is derived from Fock states exceeding this cut-off, $Q_0^2 < \mathcal{M}^2 < Q^2$. Physical quantities are independent of the intermediate cut-off Q_0; the logarithmic dependence on Q_0 cancels in the sum of intrinsic and extrinsic structure functions.

Note that the integral of xG, the momentum fraction carried by intrinsic photons, is always well-defined. In order to proceed further, we shall assume that the wave function $\psi(y, \vec{\ell}_\perp)$ is peaked at y $\simeq 1/2$. We then obtain

$$\frac{\Delta G(x, \vec{k}_\perp)}{G(x, \vec{k}_\perp)} \simeq x \left\langle \frac{1}{y} \right\rangle \simeq 2x \qquad (x \to 0) \ , \tag{14}$$

for the polarization asymmetry. We have found that this result is numerically accurate for a large range of positronium wave functions.

The opposite region (x $\to 1$), where the fermions emit hard photons, can be also readily studied. After changing variables (1 $-$ y) = (1 $-x$) (l-r), and expanding around (1 $-$ x) $\to$ 0, we obtain:

$$\begin{aligned} G^{+}(x, \vec{k}_\perp) = \frac{(1-x)}{2\pi^2\, 2(2\pi)^3} \int_0^1 d\tau \\ \Bigg\{ \left[\psi(y, \vec{\ell}_\perp) \frac{\vec{k}_\perp - \vec{\ell}_\perp}{\tau} - \psi(y-x, \vec{\ell}_\perp - \vec{k}_\perp) \frac{\vec{k}_\perp}{1-\tau} \right]^2 \\ + m^2 \left[\frac{\left| \psi(y, \vec{\ell}_\perp) \right|^2}{\tau^2} + \frac{\left| \psi(y-x, \vec{\ell}_\perp - \vec{k}_\perp) \right|^2}{(1-\tau)^2} \right] \Bigg\} \\ \times \frac{1}{\left[\frac{(\vec{\ell}_\perp - \vec{k}_\perp)^2 + m^2}{\tau} + \frac{\vec{\ell}_\perp^2 + m^2}{1-\tau} \right]^2} \ , \end{aligned} \tag{15}$$

$$G - \ (x, \vec{k}_\perp) = \frac{(1-x)^3}{2\pi^2\, 2(2\pi)^3} \int_0^1 d\tau$$

$$\left[\ \psi(y,\vec{\ell}_\perp)\ (\vec{k}_\perp - \vec{\ell}_\perp)\ -\ \psi(y-x,\ \vec{\ell}_\perp - \vec{k}_\perp)\ \vec{\ell}_\perp\ \right]^2$$

$$x\ \frac{1}{\left[\frac{(\vec{\ell}_\perp - \vec{k}_\perp)^2+m^2}{7\text{-}} + \frac{\vec{\ell}_\perp^2+m^2}{1 - r}\ \text{-}\right]^2}\ .$$

Thus the x $\rightarrow$ 1 behavior depends on the endpoint behavior of the wave function $\psi(y,\ \vec{\ell}_\perp)$. Let us assume that $\psi(y,\vec{\ell}_\perp) \sim y^p$ for y $\rightarrow$ 0, and $\sim (1\ -\ y)^q$ for $y \rightarrow 1$. If p > q, then the terms that contain $\left|\ \psi(y,\vec{\ell}_\perp)\ \right|^2$ dominate at x $\rightarrow$ 1 since y > x. This regime corresponds to the photon taking most of the longitudinal momentum of the bound state from the electron. If p < q, the terms that contain $\left|\ \psi(y-x,\vec{\ell}_\perp - \vec{k}_\perp)\ \right|^2$ will dominate, which corresponds to the photon taking its large momentum from the positron. Then

$$\begin{aligned} G^+ &= \text{constant } (1\ -\ x)^{1+2h} \\ G^- &= \text{constant } (1\ -\ x)^{3+2h} \end{aligned} \qquad (x \rightarrow\ 1)\ , \tag{16}$$

where h = $min(p,\ q)$ is the lowest endpoint power (y $\rightarrow$ 0, y $\rightarrow$ 1) behavior of $\psi(y,\vec{\ell}_\perp)$. If $\psi(y,\vec{\ell}_\perp)$ is invariant under y $\rightarrow$ (1 $-$ y), then the two endpoint powers are the same. In any case:

$$\frac{\Delta G(x,\vec{k}_\perp)}{G(x,\vec{k}_\perp)} \rightarrow 1 \qquad (x \rightarrow 1)\quad ; \tag{17}$$

i.e. the helicity of the photon tends to be aligned with that of the bound state at large x. In the case of relativistic positronium $h = 1$.[39]

We now extend this analysis to QCD bound states. A perturbative analysis is certainly justified for heavy quark systems.[40] Since the general structure of the fermion $\rightarrow$ fermion plus gluon vertices given in Table I is dictated by Lorentz invariance and parity conservation, we will assume that this perturbative structure is also applicable to light-quark systems. We thus analyze the intrinsic gluon distribution retaining only first order corrections to the valence Fock state. The appropriate color factor is obtained by the replacement of (a) by $(C_F\alpha_s)$ where C_F = $4/3$ for N_C = 3. We find similar endpoint behavior to that found in the abelian calculation. In particular, the gluon asymmetry at x $\rightarrow$ 0 is $\Delta G(x)/G(x) \simeq <1/y> x \simeq N_q x$ where N_q is the number of fermions in the valence Fock state. The x $\rightarrow$ 1 behavior for the three-quark proton can also be determined"

$$\begin{aligned} G^{+} &\sim (1-x)^4 \\ G^{-} &\sim (1-x)^6 \end{aligned} \qquad (x \to 1) \quad . \tag{18}$$

3.2. Connection with the Bound State Potential

On general grounds we expect a connection between the probability for emission (distribution function of photons or gluons) and the hyperfine interaction part of the bound state potential since both depend on the exchange of transverse gauge quanta. In fact, each diagram that contributes to the transverse potential has a corresponding cut-diagram in the expression for the distribution function. In the actual calculation, these quantities differ by just a denominator D. Thus

$$\int_0^1 dx \;\; G_{g/B} \;(x, Q_0^2) \;=\; -\left\langle \frac{\partial V}{\partial M_B^2} \right\rangle_{Q_0^2} \;, \tag{19}$$

where $G_{g/B}$ is the unpolarized distribution function of gauge fields g in the bound state B, V is the potential due to gluon exchange and self-energy corrections, and M_B is the bound-state mass. Note that the instantaneous (non-retarded) piece does not depend on M_B, so it does not contribute. As discussed above, these quantities are regulated at x $\to$ 0 by the ultraviolet cutoff Q_0^2 in the invariant mass. This singularity cancels in the hyperfine splitting:

$$\int_0 dx \;\left[\, G_{\gamma/\mathrm{ortho}\uparrow}\;(x) \;-G_{\gamma/\mathrm{para}}\;(x)\right] \;=\; -\left\langle \frac{\Delta\partial V}{\partial M_B^2} \right\rangle_{hfs} \tag{20}$$

where $\langle\;\rangle_{hfs}$ refers to the spin-dependent part of the bound state potential.

In the case of gluons in QCD bound states, we obtain analogous results:

$$\int_0 dx \;\left[\, G_{g/\rho}\;(x) \;-G_{g/\pi}\;(x)\right] \;=\; -\left\langle \frac{\Delta\partial V}{\partial M_B^2} \right\rangle_{hfs} \tag{21}$$

for mesons (ρ and π), and

$$\int_0 dx \;\left[\, G_{g/p}\;(x) \;-G_{g/\Delta}\;(x)\right] \;=\; -\left\langle \frac{\Delta\partial V}{\partial M_B^2} \right\rangle_{hfs} \tag{22}$$

for baryons (p and A).

These expressions can be analytically continued, relating the difference of fragmentation functions of gluons $D_{H/g}(z, Q^2)$ into hadrons H of different spin to the hyperfine splitting piece of the bound state potential.

3.3. Summary on the Intrinsic Gluon Distribution

The gluon distribution of a hadron is usually assumed to be generated from QCD evolution of the quark structure functions beginning at an initial scale Q_0^2.[42] In such a model there are no gluons in the hadron at a resolution scale below Q_0. The evolution is completely incoherent; i.e., each quark in the hadron radiates independently.

In the approach presented here it is recognized that the bound state wave function itself generates gluons. This is clear from the relationship between the gluon distribution and the transverse part of the bound-state potential. To the extent that gluons generate the binding, they also must appear in the intrinsic gluon distribution. We emphasize that the diagrams in which gluons connect one quark to another are not present in the usual QCD evolution equations. Evolution contributions correspond in the bound-state equation to self-energy corrections to the quark lines at resolution scales $\mathcal{M}^2 > Q_0^2$.

The model forms given in Eqs. (6) and (7) provide a convenient model for the nucleon's polarized and unpolarized intrinsic gluon distributions which takes into account coherence at low x and perturbative constraints at high x. It is expected that this should be a good characterization of the gluon distribution at the resolution scale $Q_0^2 \simeq M_p^2$.

It is well-known that the leading power at x $\sim$ 1 is increased when QCD evolution is taken into account. The change in power is[32]

$$\Delta p_g(Q^2) = 4C_A\,\zeta(Q^2, Q_0^2) = \frac{1}{\pi}\int_{Q_0^2}^{Q^2} \frac{d\kappa^2}{\kappa^2}\alpha_s(\kappa^2), \tag{23}$$

where C_A = 3 in QCD. For typical values of $Q_0 \sim 1\ GeV$, $\Lambda_{\overline{MS}} \sim 0.2\ GeV$ the change in power is moderate: $\Delta p_g(2\,GeV^2)$ = 0.28, $\Delta p_g(10\,GeV^2)$ = 0.78. A recent determination of the unpolarized gluon distribution of the proton at $Q^2 = 2\ GeV^2$ using direct photon and deep inelastic data has been given in Ref. 43. The best fit over the interval $0.05 \leq x \leq 0.75$ assuming the form $xG(x, Q^2 = 2\ GeV^2) = A(1-x)^{\eta_g}$ gives $\eta_g = 3.9 \pm 0.11(+0.8-0.6)$, where the errors in parenthesis allow for systematic uncertainties. This result is compatible with the prediction η_g = 4 for the intrinsic gluon distribution at the bound-state scale, allowing for the increase in the power due to evolution.

4. BOUND VALENCE-QUARK DISTRIBUTIONS

Deep inelastic lepton scattering and lepton-pair production experiments measure the light-cone longitudinal momentum distributions x = $(k_q^0 + k_q^z)/(p_H^0 + p_H^z)$ of quarks in hadrons through the relation

$$F_2^H(x, Q^2) = \sum_q e_q^2 x G_{q/H}(x, Q^2). \tag{24}$$

$F_2^H(x, Q^2)$ is the leading-twist structure function at the momentum transfer scale Q, Four-momentum conservation at large Q^2 then leads to the identification x = $x_{Bj} = Q^2/2p \cdot q$. In principle, the distribution functions $G_{q/H}$ could be computed from the bound state solutions of QCD.[44] For example, given the wave functions $\psi_{n/H}^{(Q)}(x_i, \vec{k}_{\perp_i}, \lambda_i)$ in the light-cone Fock expansion of the hadronic state, one can write the distribution function in the form[45]

$$G_{q/H}(x, Q^2) = \sum_{n,\lambda_i} \int \prod_{1} \frac{dx_i d^2 k_{\perp_i}}{16\pi^3} |\psi_{n/H}^{(Q)}(x_i, \vec{k}_{\perp_i}, \lambda_i)|^2 \sum_{b=q} \delta(x_b - x). \tag{25}$$

Here $x_i = k_i^+/p_H^+ = (k_i^0 + k_i^z)/(p_H^0 + p_H^z)$ is the light-cone momentum fraction of each constituent, where $\sum_i x_i = 1$ and $\sum_i k_{\perp_i} = 0$ in each Fock state *n*. The sum is over all Fock components n and helicities λ_i, integrated over the unconstrained constituent momenta.

An important concept in the description of any bound state is the definition of "valence" constituents. In atomic physics the term "valence electrons" refers to the electrons beyond the closed shells which give an atom its chemical properties. Correspondingly, the term "valence quarks" refers to the quarks which give the bound state hadron its global quantum numbers. In quantum field theory, bound states of fixed particle number do not exist; however, the light-cone expansion allows a consistent definition of the valence quarks of a hadron: the valence quarks appear in each Fock state together with any number of gluons and quark–anti-quark pairs; each component thus has the global quantum numbers of the hadron.

How can one identify the contribution of the valence quarks of the bound state with the phenomenological structure functions? Traditionally, the distribution function $G_{q/H}$ has been separated into "valence" and "sea" contributions:[46] $G_{q/H}$ =

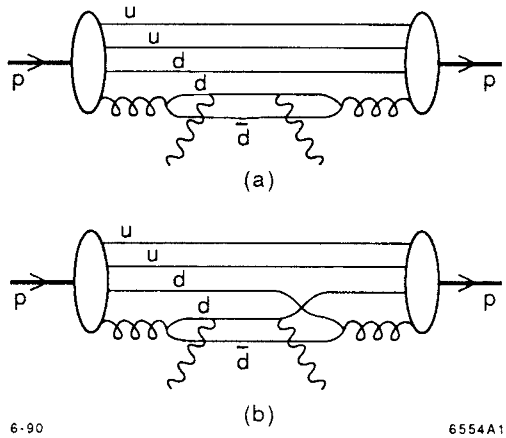

Figure 4. Structure function contributions from the three–quark plus one pair Fock state of the proton. The $d\bar{d}$ pair in diagram (a) contributes to the sea distribution, but diagram (b) due to anti–symmetrization of the d–quarks cannot be separated uniquely into "valence" versus "sea" parts.

$G^{\rm val}_{q/H} + G^{\rm sea}_{q/H}$, where, as an operational definition, one assumes

$$G^{\rm sea}_{q/H}(x, Q^2) = G^{\rm sea}_{\bar{q}/H}(x, Q^2), \qquad (0 < x < 1), \tag{26}$$

and thus $G^{\rm val}_{q/H}(x, Q^2) = G_{q/H}(x, Q^2) - G_{\bar{q}/H}(x, Q^2)$. The assumption of identical quark and anti-quark sea distributions is reasonable for the s and $\bar{s}$ quarks in the proton. However, in the case of the u and d quark contributions to the sea, anti–symmetrization of identical quarks in the higher Fock states implies non-identical q and $\bar{q}$ sea contributions. This is immediately apparent in the case of atomic physics, where Bethe–Heitler pair production in the field of an atom does not give symmetric electron and positron distributions since electron capture is blocked in states where an atomic electron is already present. Similarly in QCD, the $q\bar{q}$ pairs which arise from gluon splitting as in Fig. 4(a) do not have identical quark and anti-quark sea distributions; contributions from interference diagrams such as Fig. 4(b), which arise from the anti-symmetrization of the higher Fock state wave functions, must be taken into account. Although the integral of the conventional valence distribution gives correct charge sum rules, such as $\int_0^1 dx(G_{q/H}(x) - G_{\bar{q}/H}(x))$, it can give a misleading reading of the actual momentum distribution of the valence quarks. It is also interesting to notice that the Gottfried sum rule assumes the equality of anti-up and anti-down quarks in the proton. Because of the stronger Pauli blocking of up quarks, however, one would expect a relative suppression of anti-up quarks in the proton, giving an important correction to the sum rule.

The standard definition also has the difficulty that the derived valence quark distributions are apparently singular in the limit $x \to 0$. For example, standard phenomenology indicates that the valence up-quark distribution in the proton behaves as $G^{\rm val}_{u/p} \sim x^{-\alpha_R}$ for small x[47,46] where $\alpha_R \approx 0.5$.[48] This implies that quantities that depend on the < 1/x > moment of the valence distribution diverge. This is the case for the "sigma term" in current algebra and the $J = 0$ fixed pole in Compton scattering.[49] Furthermore, it has been shown[50] that the change in mass of the proton when the quark mass is varied in the light-cone Hamiltonian is given by an extension of the Feynman-Hellmann theorem:

$$\frac{\partial M_p^2}{\partial m_q^2\ (Q^2)} = \int_0^1 \frac{dx}{x}\, G_{q/p}\,(x, Q^2). \tag{27}$$

In principle, this formula allows one to compute the contribution to the proton–neutron mass difference due to the difference of up and down quark masses. However, again, with the standard definition of the valence quark distribution, the integration is undefined at low x. Even more seriously, the expectation value of the light-cone kinetic energy operator

$$\int_0^1 dx\, \frac{< k_\perp^2 > + m^2}{x}\, G_{q/p}(x, Q). \tag{28}$$

is infinite for valence quarks if one uses the traditional definition. There is no apparent way of associating this divergence of the kinetic energy operator with renormalization.[51] Notice that a divergence at x = 0 is an ultraviolet infinity for a massive quark, since it implies $k^+ = k^0 + k^z = 0$; i.e. $k^z \to -\infty$. A bound state wave function would not be expected to have support for arbitrarily large momentum components.

Part of the difficulty with identifying bound state contributions to the proton structure functions is that many physical processes contribute to the deep inelastic lepton-proton cross section: From the perspective of the laboratory or center of mass frame, the virtual photon can scatter out a bound-state quark as in the atomic physics photoelectric process, or the photon can first make a $q\overline{q}$ pair, either of which can interact in the target. As we emphasize here, in such pair-production processes, one must take into account the Pauli principle which forbids creation of a quark in the same state as one already present in the bound state wave function. Thus the lepton interacts with quarks which are both intrinsic to the proton's bound-state structure, and with quarks which are extrinsic; i.e. created in the electron-proton collision itself. Note that such extrinsic processes would occur in electroproduction even if the valence quarks had no charge. Thus much of the phenomena observed in electroproduction at small values of x, such as Regge behavior, sea distributions associated with photon-gluon fusion processes, and shadowing in nuclear structure functions should be identified with the extrinsic interactions, rather than processes directly connected with the proton's bound-state structure.

In Ref. 11 Ivan Schmidt and I propose a definition of "bound valence-quark" distribution functions that correctly isolates the contribution of the valence constituents which give the hadron its flavor and other global quantum numbers. In this new separation, $G_{q/p}(x, Q^2) = G^{\rm BV}_{q/p}(x, Q^2) + G^{\rm NV}_{q/p}(x, Q^2)$, non-valence quark distributions are identified with the structure functions which would be measured if the valence quarks of the target hadron had zero electro-weak charge. We shall prove that with this new definition the bound valence-quark distributions $G^{\rm BV}_{q/p}(x, Q^2)$ vanish at $x \to 0$, as expected for a bound-state constituent.

4.1. Construction of Bound Valence-Quark Distributions

In order to construct the bound valence-quark distributions, we imagine a *gedanken* QCD where, in addition to the usual set of quarks $\{q\} = \{u, d, s, c, b, t\}$, there is another set $\{q_0\} = \{u_0, d_0, s_0, c_0, b_0, t_0\}$ with the same spin, masses, flavor, color, and other quantum numbers, except that their electromagnetic charges are zero.

Let us now consider replacing the target proton p in the lepton-proton scattering experiment by a chargeless proton p_0 which has valence quarks q_0 of zero electromagnetic charge. In this extended QCD the higher Fock wave functions of the proton p and the chargeless proton p_0 both contain $q\overline{q}$ and $q_0\overline{q_0}$ pairs. As far as the strong QCD interactions are concerned, the physical proton and the *gedanken* chargeless proton are equivalent.

We define the bound valence-structure function of the proton from the difference between scattering on the physical proton minus the scattering on the chargeless proton, in analogy to an "empty target" subtraction:

$$F_i^{\rm BV}(x, Q^2) \equiv F_i^{p}(x, Q^2) - F_i^{p_0}(x, Q^2). \tag{29}$$

The non-valence distribution is thus $F_i^{\rm NV}(x, Q^2) = F_i^{p_0}(x, Q^2)$. The $F_i(x, Q^2)$ $(i = 1, 2,)$ are the leading-twist structure functions, with $F^{\rm BV}_{2H}(x, Q^2) = \sum_q e_q^2 x G^{\rm BV}_{q/H}(x, Q^2)$, etc. The situation just described is similar to the atomic physics case, where in order to correctly define photon scattering from a bound electron, one must subtract the cross section on the nucleus alone, without that bound electron present.[52] Physically the nucleus can scatter photons through virtual pair production, and this contribution has to be subtracted from the total cross section. In QCD we cannot construct protons without the valence quarks; thus we need to consider hadrons with chargeless valence constituents.[53]

Notice that the cross section measured in deep inelastic lepton scattering on p_0 is not zero. This is because the incident photon (or vector boson) creates virtual $q\overline{q}$ pairs which scatter strongly in the gluonic field of the chargeless proton target. In fact at small x the inelastic cross section is dominated by J = **1** gluon exchange contributions, and thus the structure functions of the physical and chargeless protons become equal:

$$\lim_{x\to 0}\left[F_i^p(x,Q^2)-F_i^{p_0}(x,Q^2)\right] = 0 . \tag{30}$$

Remarkably, as we show below, the bound valence-quark distribution function $G^{BV}_{q/H}$ vanishes at x $\to$ 0; it has neither Pomeron x^{-1} nor Reggeon $x^{-\alpha_R}$ contributions.

Although the *gedanken* subtraction is impossible in the real world, we will show that, nevertheless, the bound valence-distribution can be analytically constrained at small x_{bj}. This opens up the opportunity to extend present phenomenology and relate measured distributions to true bound state wave functions.

In the following sections we will analyze both the atomic and hadronic cases, paying particular attention to the high energy regime.

4.2. Atomic Case

Since it contains the essential features relevant for our discussion, we will first analyze photon scattering from an atomic target. This problem contains an interesting paradox which was first resolved by Goldberger and Low in 1968.[52] Here we give a simple, but explicit, derivation of the main result.

The Kramers-Kronig dispersion relation relates the forward Compton amplitude to the total photo-absorptive cross section[54]

$$f(k) - f(0) = \frac{k^2}{2\pi^2}\int_0^\infty dk' \frac{\sigma(k')}{k'^2 - k^2 - i\epsilon}, \tag{31}$$

where k is the photon energy. One should be able to apply this formula to scattering on a bound electron (e_b) in an atom. However, there is an apparent contradiction. On the one hand, one can explicitly compute the high energy $\gamma e_b \to \gamma e_b$ forward amplitude: it tends to a constant value at $k \to \infty$, the electron Thomson term, $f(k) \to -e^2/m_b^e$, where m_b^e is the effective electron mass corrected for atomic binding.[55] On the other hand, the $\mathcal{O}\left(e^2\right)$ cross section for the photoelectric effect

$\gamma e_b \to$ e' behaves as $\sigma_{\text{photo}} \sim 1/k$ at high energies. But then the integral in the dispersion relation predicts logarithmic behavior for $f(k)$ at high energy in contradiction to the explicit calculation. Evidently other contributions to the inelastic cross-section cannot resolve this conflict.

This problem was solved[52] by carefully defining what one means by scattering on a bound state electron. For both the elastic Compton amplitude and the inelastic cross section one must subtract the contribution in which the photon scatters off the Coulomb field of the nucleus (empty target subtraction). Thus $a(k)$ in the Kramers-Kronig relation is really the difference between the total atomic cross section $\sigma_{\text{atom}}(k)$ and the nuclear cross section $\sigma_{\text{nucleus}}(k)$, which is dominated by pair production. We will present a simple proof that the high energy behavior $\sim 1/k$ of the cross sections exactly cancels in this difference, which is a necessary condition for a consistent dispersion relation.

The total cross section for photon scattering on the atom is dominated by two main terms: the photoelectric contribution and e^+e^- pair production, with the produced electron going into a different state than the electron already present in the atom.[56] On the other hand, in the subtraction, pair production in the field of the-nucleus is not restricted by the Pauli principle; this cross section contains a contribution where the produced electron goes into the same state as the bound state electron of the atom, plus other terms in which it goes into different states. These last contributions cancel in the difference $\sigma_{\text{atom}} - \sigma_{\text{nucleus}}$. Thus the bound-state electron photo-absorption cross section is the difference between the photoelectric cross section on the atom and the pair production *capture* cross section on the nucleus, where the produced electron is captured in the same state as the original bound state electron: $\sigma_{e_b} = \sigma_{\text{photoelectric}} - \sigma_{\text{capture}}$. This is depicted graphically in Fig. 5.

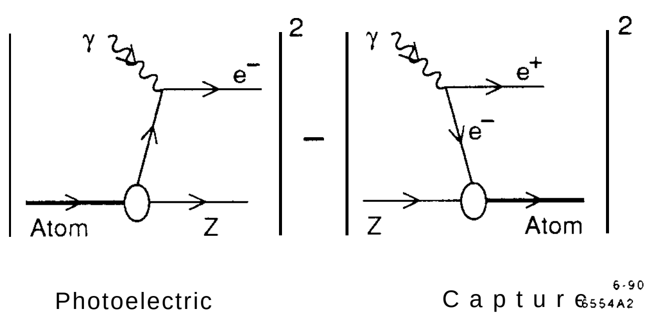

Figure 5. The bound–electron photo–absorption cross section $\sigma_{\gamma e_b}$ is defined as the difference of $\gamma - Atom$ and $\gamma - Nucleus$ cross sections. This can also be expressed as the difference between the atomic "photoelectric" cross section and the pair production "capture" cross section on the nucleus, but with the produced electron going into the same atomic state as the original bound state electron.

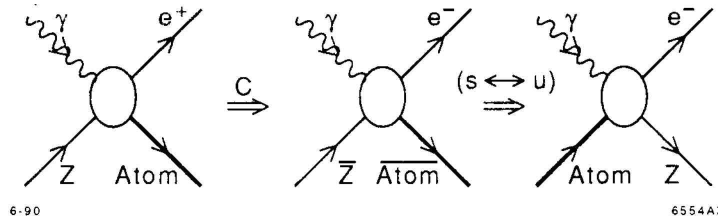

Figure 6. The helicity–summed squared amplitude for the process $\gamma Z \to e^+ Atom$ is equal, by charge conjugation, to the helicity–summed squared amplitude for $\gamma \overline{Z} \to e^- \overline{Atom}$, up to a phase. This is also equal by crossing to the helicity–summed squared amplitude for the process $\gamma Atom \to e^- Z$, but with s and u interchanged.

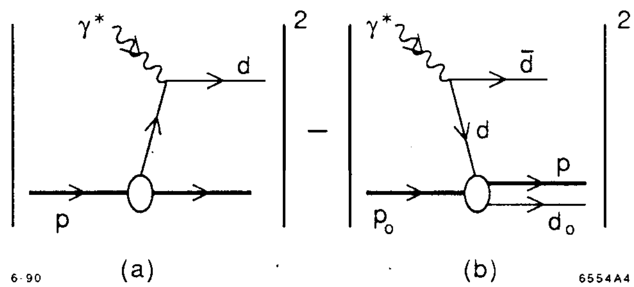

Figure 7. The bound valence–quark distribution of quark d can be calculated from the difference between (a) the cross section on the state p in which the virtual photon momentum is absorbed by the quark d, and (b) the $d\bar{d}$ pair production cross section in the field of p_0, but with the produced d quark ending in the same state as the d quark in the original proton state p.

We next note that the squared amplitude for the capture process $\gamma Z \to e^+ Atom$ is equal, by charge conjugation, to the squared amplitude for $\gamma \overline{Z} \to$ e-$\overline{\text{Atom}}$. (See Fig. 6.) Furthermore, by crossing symmetry, the (helicity summed) squared amplitude for this last process is equal to the (helicity summed) squared amplitude for $\gamma Atom \to$ e-2, with p_Z and $(-p_{\text{Atom}})$ interchanged. This is equivalent to the interchange of the Mandelstam variables $s = (p_\gamma + p_Z)^2$ and $u = (p_\gamma - p_{\text{Atom}})^2$. Thus at high photon energies (where $s \simeq -u$), the two cross sections $\sigma_{\text{photoelectric}}$ and σ_{capture} of Fig. 5 cancel, consistent with the Kramers–Kronig relation. In Regge language, the imaginary part of the $J = 0$ Compton amplitude is zero.

The proof we have presented implicitly assumes the equality of the flux factors for the photoelectric process on the atom and the capture process on the nucleus. This is normally a good approximation since the atomic and nuclear masses are almost identical for $M_Z >> m$,. However, for finite mass systems such as muonic atoms, the mass of the nucleus and atom are unequal, and the cross sections do

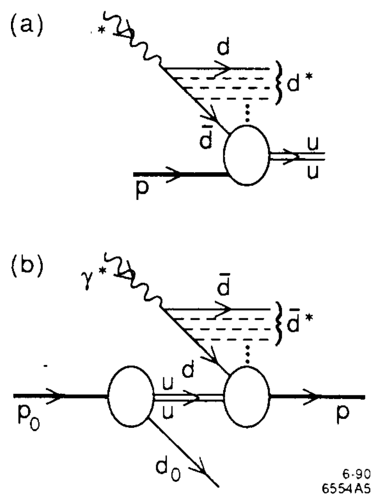

Figure 8. Amplitudes describing Reggeon behavior at small x (a) in electroproduction, and (b) in the subtraction term of Fig. 7(b).

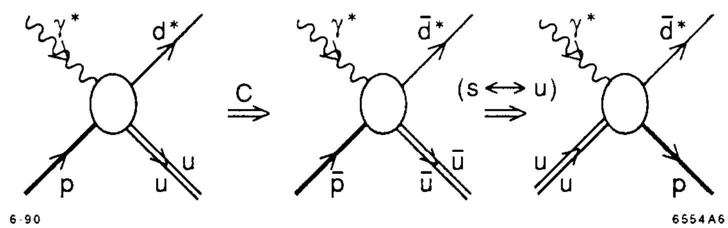

Figure 9. The helicity–summed squared amplitude for (a) $\gamma^* p \to d^*(uu)$ is equal, by charge conjugation, to the helicity–summed squared amplitude for the process (b) $\gamma^* \overline{p} \to \overline{d}^*(\overline{uu})$, up to a phase. This is also equal, by crossing symmetry, to the helicity–summed squared amplitude for (c) $\gamma^*(uu) \to \overline{d}^* p$, with s and u interchanged. Thus at high energies the Reggeon contribution from the subtraction term of Fig. 8(b) cancels the Reggeon contribution of Fig. 8(a).

not cancel at high energy. The difficulty in this case is that the nucleus does not provide the correct "empty target" subtraction.

However, we can extend the analysis to the general atomic problem by considering hypothetical atoms A_0 consisting of null leptons ℓ_0 with normal electromagnetic and Coulomb interactions with the nucleus but with zero external charge. [In effect, we consider an extended QED with U(1) x U(1) gauge interactions, where the null lepton has charge (-1, 0), and the normal lepton and nucleus have charges (-1, -1) and (Z, Z), respectively.] The empty target subtraction is defined as the difference between the cross section on the normal atom $A = (Z\ell)$ and the cross section on the null atom $A_0 = (Z\ell_0)$. Since the mass and binding interactions of A

and A_0 are identical, the photo-absorption flux factors are the same in both cases.

As in the earlier proof, the matrix element for the photoelectric process on the atom A becomes equal in modulus at high energies with the matrix element for the capture process on the null atom A_0. Note that in the computation of the capture process amplitude, the presence of the spectator lepton ℓ_0 is irrelevant since it remains in the original quantum state (say $1S$): The required matrix element of the current is

$$\left\langle A\ell_0(1S)\ell^+|J^\mu|A_0\right\rangle = \left\langle A\ell_0(1S)\ell^+|\overline{\psi}_\ell\gamma^\mu\psi_\ell b^\dagger_{\ell_o}(1S)|Z\right\rangle = \left\langle A\ell^+|J^\mu|Z\right\rangle .$$

By charge conjugation and crossing this is equal in modulus to

$$\left\langle Z\ell^-|J^\mu|A\right\rangle ,$$

the corresponding photoelectric matrix element with s $\rightarrow$ u. Final-state interactions can only affect the phase at high energies. Thus we obtain cancellation of the photoelectric and capture cross sections at high energies, and verify the Kramers–Kronig dispersion relation for Compton scattering on leptons bound to finite mass nuclei.

4.3. Reggeon Cancellations in QCD

We now return to the analysis of the "bound valence-quark distributions" of the proton. According to the discussion of Section 4.1, the measurement of the bound valence-quark distribution requires an "empty target" subtraction:

$$\sigma(\gamma^* p \rightarrow X) - \sigma(\gamma^* p_0 \rightarrow X).$$

Both p and p_0 contain higher Fock states with arbitrary number of gluons, $q\overline{q}$, and $q_0\overline{q_0}$ pairs. It is clear that the terms associated with $J \approx 1$ Pomeron behavior due to gluon exchange cancel in the difference. In this section we shall prove that the Reggeon terms also cancel, and thus the resulting distribution of bound valence quarks $G^{\rm BV}_{q/p}(x, Q^2)$ vanishes as $x \rightarrow 0$.

As in the atomic case, we now proceed to describe the leading contributions to the scattering of a photon from both the proton p and the state p_0. For simplicity of notation, we will consider an example which isolates just the bound valence d-quark distribution of the proton $p(uud)$; in this case the subtraction term is the deep inelastic cross section on the system $p_0(uud_0)$ in which the d_0 valence quark has normal QCD interactions but does not carry electric charge. The general case, where the subtraction is on the completely neutral state $p_0(u_0u_0d_0)$, is a simple generalization. The high Q^2 virtual photo-absorption cross section on the proton (laboratory frame) contains two types of terms: contributions in which a quark in p absorbs the momentum of the virtual photon; and terms in which a $q\overline{q}$ pair is created, but the produced q is in a different quantum state than the quarks already present in the hadron. On the other hand, the cross section for scattering of the virtual photon from the state $p_0(uud_0)$ contains contributions that differ from the $p(uud)$ case in two important aspects: first the virtual photon can be absorbed only by charged quarks; and in $d\overline{d}$ pair production on the null proton p_0, the d quark can be produced in any state. Thus the difference between the cross sections off p and p_0 equals a term analogous to $\sigma_{\text{photoelectric}}$, in which a d quark in p absorbs the photon momentum, minus a $d\overline{d}$ pair production contribution on p_0 analogous to σ_{capture}, in which the produced d quark ends up in the same quantum state as the d quark in the original proton state p. This is shown graphically in Fig. 7.[57]

Reggeon behavior in the electroproduction cross section can be understood as due to the appearance of a spectrum of bound $q\overline{q}$ states in the t-channel. The absorptive cross section associated with t-channel ladder diagrams is depicted in Fig. 8(a). The summation of such diagrams leads to Reggeon behavior of the deep inelastic structure functions at small x.[58] In the rest system, the virtual photon creates a $d\overline{d}$ pair at a distance proportional to $1/x$ before the target. The radiation which occurs over this distance contributes to the physics of the Reggeon behavior.

A corresponding Reggeon contribution at low x also occurs in the subtraction term indicated in Fig. 8(b). In the case of the proton target, the d-quark, after radiation, cannot appear in the quantum state already occupied by the d-quark in the proton because of the Pauli principle. However, the corresponding contribution is allowed on the p_0 target: in effect, the d-quark replaces the do-quark and is captured into a proton. The capture cross section is computed from the amplitude for $\gamma^* p_0 \rightarrow \overline{d}^* p\, d_0^{1S}$.[59] As in the corresponding atomic physics analysis, the spectator d_0 quark in the null target p_0 is inert and cancels out from the amplitude. Thus we only need to consider effectively the (helicity summed) squared amplitude for $\gamma^*(uu) \rightarrow \overline{d}^* p$. However, as illustrated in Fig. 9 this amplitude, after charge conjugation and crossing s $\rightarrow$ u, is equal to the (helicity summed) $\gamma^* p \rightarrow d^*(uu)$ squared amplitude at small x. The flux factors for the proton and null proton target are equal.

If we write $s\sigma_{\text{photoelectric}}$ as a sum of Regge terms of the form $\beta_R\,|s\,|^{\alpha_R}$, where $\alpha_R > 0$ then the subtraction of the capture cross section on the null proton will give the net virtual photo-absorption cross section as a sum of terms $s\sigma^{\text{BV}} = \sum_R \beta_R(|s|^{\alpha_R} - |u|^{\alpha_R})$. If we ignore mass corrections in leading twist, then s $\simeq Q^2(1-x)/x$ and u $\simeq -Q^2/x$. Thus for small x every Regge term is multiplied by a factor $K_R = (-\alpha_R)x$. For example, for $\alpha_R = 1/2$ (which is the leading even charge-conjugation Reggeon contribution for non-singlet isospin structure functions), $F_2^{p(uud)} - F_2^{p_0(uud_0)} \sim x^{3/2}$. The bound valence-quark non-singlet (I = 1) distribution thus has leading behavior $G^{\rm BV}_{q/H} \sim x^{1/2}$ and vanishes for $x \rightarrow 0$.

We can also understand this result from symmetry considerations. We have shown from crossing symmetry $G_{q/p}(x, Q^2) - G_{\overline{q}/p_0}(x, Q^2) \rightarrow 0$ at low x. Thus the even charge-conjugation Reggeon and Pomeron contributions decouple from the bound valence-quark distributions.

The analytic cancellation of the leading Reggeon contributions of the s-channel and u-channel contributions suggests that, given sufficiently detailed Regge fits to the data for the non-singlet structure functions, one could construct a phenomenological model for the bound valence-quark distributions. Eventually, lattice gauge theory or other non-perturbative methods for solving QCD, such as discretized light-cone quantization,[44] may provide detailed first-principle predictions for the bound valence-quark distributions which could be compared with the phenomenological forms.

4.4. Summary on Bound-Valence Quark Distributions

The observation that the deep inelastic lepton-proton cross section is non–zero, even when the quarks in the target hadron carry no charge, implies that we should distinguish two separate contributions to deep inelastic lepton scattering: intrinsic (bound-state) and *extrinsic* (non-bound) structure functions. The extrinsic contributions are created by the virtual strong interactions of the lepton itself, and are present even if the quark fields of the target are chargeless. The bound valence-quark distributions, defined by subtracting the distributions for a gedanken "null" hadron with chargeless valence quarks, correctly isolates the valence-quark contributions intrinsic to the bound-state structure of the target. As we have shown, both the Pomeron and leading Reggeon contributions are absent in the bound valence-quark distributions. The leading Regge contributions are thus associated with particles created by the photon-hadron scattering reaction, processes extrinsic to the bound state physics of the target hadron itself. The bound valence-quark distributions are in principle computable by solving the bound state problem in QCD. Sum rules for the proton derived from properties of the hadronic wave function thus apply to the bound valence-quark contributions. In particular, the light-cone kinetic energy of the bound valence-quarks,

$$\int_0^1 dx \, \frac{< k_\perp^2 > + m^2}{x} \, G^{\rm BV}_{q/p}(x, Q) \tag{32}$$

is finite, as expected for a bound state wave function contribution. The ultraviolet divergence of the kinetic energy obtained from the non-valence distribution is associated with the production of high mass states in the electron-proton collision, rather than the distribution of the bound-state valence quarks.

The essential reason why the new definition of the bound valence-quark distribution differs from the conventional definition of valence distributions is the Pauli principle: the anti-symmetrization of the bound state wave function for states which contain quarks of identical flavor. As we have shown, this effect plays a dynamical role at low x, eliminating leading Regge behavior in the bound valence-quark distributions. In the atomic physics case, where the leading Regge behavior corresponds to $J = \alpha_R = 0$, the analogous application of the Pauli principle leads to analytic consistency with the Kramers-Kronig dispersion relation for Compton scattering on a bound electron.

5. INTRINSIC CHARM-QUARK DISTRIBUTIONS

There are a number of striking anomalies in the data[60] for charm production which cannot be readily explained by conventional leading twist $gg \rightarrow c\overline{c}$ or $q\overline{q} \rightarrow c\overline{c}$ fusion subprocesses. The first signals for charm baryon production at large x_F were reported by the BCF and other groups at the ISR. The results are reviewed in Ref. 60. Other anomalies include:

1. The EMC data[61] for the charm structure function of the nucleon appears to be too high at large x_{Bj}.
2. The LEBC bubble chamber data[62] for charm production in pp collisions indicates an excess of D events at large x_F. The excess is not associated with D's that contain the proton's valence quark.
3. The cross section measured by the WA-62 group[63] for C-N $\rightarrow \Xi(csu)X$ is too large and flat at large x_F.
4. The NA-3 data[25] for J/ψ production in pion-nucleus and proton-nucleus collisions can be represented as two components: a normal contribution in the central region which is almost additive in nuclear number that can be accounted for by $gg \rightarrow c\overline{c}$ and $q\overline{q} \rightarrow c\overline{c}$ fusion, and a second "diffractive contribution" which dominates at large x_F and is strongly shadowed. This last contribution suggests that high momentum $c\overline{c}$ systems are being produced on the front surface of the nuclear target.

It is difficult to understand any of these anomalies, particularly the production of high x_F charmonium unless the proton itself has an intrinsic charm contribution[64] to its structure function. From the perturbative point of view, a $uudc\overline{c}$

Fock component can be generated by the gg $\rightarrow c\bar{c}$ amplitude where the gluons are emitted from two of the valence quarks. The probability for finding the heavy quark pair of mass $M_{Q\overline{Q}}$ or greater is thus of order $\alpha_s^2\ (M^2_{Q\overline{Q}})/M^2_{Q\overline{Q}}$ (see the introduction). Intrinsic charm is thus a higher twist mechanism. The leading twist extrinsic charm contributions depend on the logarithm of the heavy quark mass. Since the intrinsic charm quarks are associated with the bound-state equation for the proton, then all the partons tend to have equal velocity. Unlike normal sea quarks generated by evolution, this implies that the heaviest constituents, the intrinsic charm quarks, will take a large fraction of the proton's momentum. In a hadronic collision the c and $\bar{c}$ can coalesce to produce a charmonium state with the majority of the proton's momentum.[65] The EMC charm structure function data requires a 0.3 % probability for the intrinsic charm Fock state in the nucleon.?

According to the hard scattering picture of QCD, production cross sections involving large momentum transfer should factorize and be approximately additive in the nucleon number, $d\sigma_A = A^{\alpha}(x_F, p_T) d\sigma_N$ with $\alpha \sim 1$, up to the small shadowing and anti-shadowing corrections seen in deep inelastic lepton-nucleus scattering. (See Section 6.) In the Drell-Yan process, large mass muon pair production, $\alpha \simeq 1$ for all x_F is indeed observed? However, several experiments on open charm production show[60] that $\alpha(x_F \geq 0.2) \simeq 0.7..\,.0.8$. For small x_F, an indirect analysis[62] comparing different measurements of the total charm production cross section indicates $\alpha(x_F \simeq 0) \simeq 1$.

The most detailed data on the nuclear dependence of charm production is available from the hadroproduction of J/ψ. Here a decrease of α from $\alpha(x_F \simeq 0) \simeq 1$ to $\alpha(x_F \simeq 0.8) \simeq 0.8$ has been seen by several groups.[67] The analysis of Badier, et *al.*[25] is particularly interesting. They noted that the production of J/ψ at large x_F (up to $x_F \simeq 0.8$) cannot be explained by the gluon and light quark fusion mechanisms of perturbative QCD, due to the anomalous A-dependence. However, their π-$A \rightarrow J/\psi + X$ data was well reproduced if, in addition to hard QCD fusion (with $\alpha = 0.97$), they included a "diffractive" component of J/ψ production at high x_F with $\alpha = 0.77$. Using their measured A-dependence to extract the "diffractive" component, they found that (for a pion beam) that the J/ψ distribution peaks at $x_F \simeq 0.5$ and dominates the hard scattering A' component for x ≥ 0.6. The anomalous nuclear dependence cannot be explained by gluon shadowing since the data scale in x_F rather than the gluon momentum fraction in the nucleus x_2.[68] Final state absorption of the charmonium state would predict an increasing nuclear yield with J/ψ momentum, opposite what is seen. Furthermore, this would not explain the similar A-dependence observed by E–772[26] for J/ψ and ψ' production.

A diffractive contribution to heavy quarkonium production is consistent with QCD when one takes into account the higher twist intrinsic charm component of the projectile wave function. In high energy hadron-nucleus collisions the nucleus may be regarded as a "filter" of the hadronic wave function.[3] The argument, which relies only on general features such as time dilation, goes as follows.[69] As discussed in the introduction, one can define a Fock state expansion of a hadron in terms of its quark and gluon constituents; e.g. for a meson,

$$|h\rangle = \mathrm{Id} + |q\bar{q}g\rangle + |q\bar{q}q\bar{q}\rangle + \ldots \tag{33}$$

The various Fock components will mix with each other during their time evolution. However, at sufficiently high hadron energies E_h, and during short times t, the mixing is negligible. Specifically, the relative phase $\exp[-i(E - E_h)t]$ of a given term in Eq. (33) is proportional to the energy difference

$$E - E_h = \left[\sum_i \frac{m_i^2 + \mathbf{p}_{Ti}^2}{x_i} - M_h^2\right] \Big/ (2E_h) \tag{34}$$

which vanishes for $E_h \to \infty$. Hence the time evolution of the Fock expansion is, at high energies, diagonal during the time $\sim 1/R$ it takes for the hadron to cross a nucleus of radius R.

The diagonal time development means that it is possible to describe the scattering of a hadron in a nucleus in terms of the scattering of its individual Fock components. Let us explore the consequences for typical, soft collisions characterized by momentum transfers $q_T \simeq \Lambda_{QCD}$. The partons of a given Fock state will scatter independently of each other if their transverse separation is $r_T \geq 1/\Lambda_{QCD}$; *i.e.* if the state is of typical hadronic size. Conversely, the nuclear scattering will be coherent over the partons in Fock states having $r_T << 1/\Lambda_{QCD}$ since $e^{iq_T \cdot r_T} \simeq 1$. For color-singlet clusters, the interference between the different parton amplitudes interacting with the nuclear gluonic field is destructive. Thus the nucleus will appear nearly transparent to small, color-singlet Fock states. In an experiment detecting fast secondary hadrons the nucleus indeed serves, then, as a filter that selects the small Fock components in the incident hadrons.

Now consider the intrinsic charm state $|u\bar{d}c\bar{c}\rangle$ of a $|\pi^+\rangle$. Because of the large charm mass m_c, the energy difference in denominator of the wave function will be minimized at equal parton velocity; i.e. when the charm quarks carry most of the longitudinal momentum. Moreover, because m_c is large, the transverse momenta p_{Tc} of the charm quarks range up to $\mathcal{O}(m_c)$, implying that the transverse size of the $c\bar{c}$ system is $\mathcal{O}(1/m_c)$. Hence, provided only that the $c\bar{c}$ forms a color singlet, it can penetrate the nucleus with little energy loss. Thus the high momentum small transverse size $c\bar{c}$ color-singlet cluster in the incident hadron passes through the nucleus undeflected, and it can then evolve into charmonium states after transiting the nucleus." In effect, the nucleus is transparent to the heavy quark pair component of the intrinsic state. The remaining cluster of light quarks in the intrinsic charm Fock state has a larger transverse size and tends to be absorbed on the front surface of the nucleus. This justifies the analysis of Badier *et* al. in which the perturbative and non-perturbative charm production mechanisms were separated on the basis of their different A-dependence (α = 0.97 and α = 0.77 for a pion beam, respectively). The effective x_F–dependence of α seen in charm production is explained by the different characteristics of the two production mechanisms. Hard, gluon fusion production dominates at small x_F, due to the steeply falling gluon structure function. The contribution from intrinsic charm Fock states in the beam peaks at higher x_F, due to the large momentum carried by the charm quarks. This two-component hard-scattering plus intrinsic charm model also explains why the nuclear dependence of J/ψ production depends on x_F rather than x_2, as predicted by leading twist factorization.?

An important consequence of this picture is that all final states produced by a penetrating intrinsic $c\bar{c}$ component will have the same A-dependence. Thus, in particular, the $\psi(2S)$ radially excited state will behave in the same way as the J/ψ, in spite of its larger size. This prediction is confirmed by the recent E–772 data.[26] The nucleus cannot influence the quark hadronization which (at high energies) takes place outside the nuclear environment.

Quarkonium production due to the intrinsic heavy quark state will fall off rapidly for p_T greater than M_Q, reflecting the fast-falling transverse momentum dependence of the higher Fock state wave function. Thus we expect the conventional fusion contributions to dominate in the large p_T region. The data are in fact consistent with a simple A^1 law for J/ψ production at large p_T. The CERN experiment of Badier *et al.*[25] finds that the ratio of nuclear cross sections is close to additive in A for all x_F when p_T is between 2 and 3 GeV. The data of the FermiLab experiment of Katsanevas *et al.*[67] shows consistency with additivity for p_T ranging from 1.2 to 3 GeV.

As was discussed above, the probability for intrinsic heavy quark states in a light hadron wave function is expected[64,71] to scale up to logarithms inversely as the square of the heavy quark mass. This implies a production cross section proportional to $1/M_Q^4$. The total rate of heavy quark production by the intrinsic mechanism therefore decreases with quark mass relative to the leading-twist cross section which is proportional to $1/M_Q^2$. At large x the intrinsic production should still dominate, however, implying a nuclear dependence in this region characterized by $\alpha \simeq 0.7 \ldots 0.8$. The recent E-772 data[26] for the hadroproduction of the upsilon suggests that intrinsic beauty contributions may also be playing a role.

Experimental measurements of beauty hadroproduction in nuclei over the whole range of x will be essential for unraveling the two components of the cross section.

6. SHADOWING AND ANTI-SHADOWING OF NUCLEAR STRUCTURE FUNCTIONS

The shadowing and anti-shadowing of deep inelastic nuclear structure functions refers to the depletion of the effective number of nucleons F_2^A/F_2^N at low x $\lesssim$ 0.1, and the increase above nucleon additivity at x $\sim$ 0.15. Results from the EMC collaboration[72] and SLAC[73] indicate that the effect is roughly Q^2–independent; *i.e.* shadowing is a leading twist in the operator product analysis. In contrast, the shadowing of the real photo-absorption cross section due to p-dominance[74–77] falls away as an inverse power of Q^2.

Shadowing is a destructive interference effect which causes a diminished flux and interactions in the interior and back face of the nucleus. The Glauber analysis[78] corresponds of hadron-nucleus scattering to the following: the incident hadron scatters elastically on a nucleon N_1 on the front face of the nucleus. At high energies the phase of the amplitude is imaginary. The hadron then propagates through the nucleus to nucleon N_2 where it interacts inelastically. The accumulated phase of the hadron propagator is also imaginary, so that this two-step amplitude is coherent and opposite in phase to the one-step amplitude where the beam hadron interacts directly on N_2 without initial-state interactions. Thus the target nucleon N_2 sees less incoming flux: it is shadowed by elastic interactions on the front face of the nucleus. If the hadron-nucleon cross section is large, then for large A the effective number of nucleons participating in the inelastic interactions is reduced to $\sim A^{2/3}$, the number of surface nucleons.

In the case of virtual photo-absorption, the photon converts to a $q\overline{q}$ pair at a distance before the target proportional to w = $x^{-1} = 2p \cdot q/Q^2$ in the laboratory frame." In a physical gauge, such as the light-cone A^+ = 0 gauge, the final-state interactions of the quark can be neglected in the Bjorken limit, and effectively only the anti-quark interacts. The nuclear structure function F_2^A producing quark q can then be written as an integral[80,49] over the inelastic cross section $\sigma_{\overline{q}A}(s')$ where s' grows as l/x for fixed space-like anti-quark mass. Similarly, the anti-quark nuclear structure function is related to inelastic quark-nucleus scattering. Thus the A-dependence of the deep inelastic nuclear structure functions cross section reflects the A-dependence of the q and $\overline{q}$ cross sections in the nucleus. Hung Jung Lu and I have recently applied the standard Glauber multi-scattering theory, to $\sigma_{\overline{q}A}$ and σ_{qA} assuming that formalism can be taken over to off-shell interactions.' The shadowing mechanism is illustrated in Fig. 10.

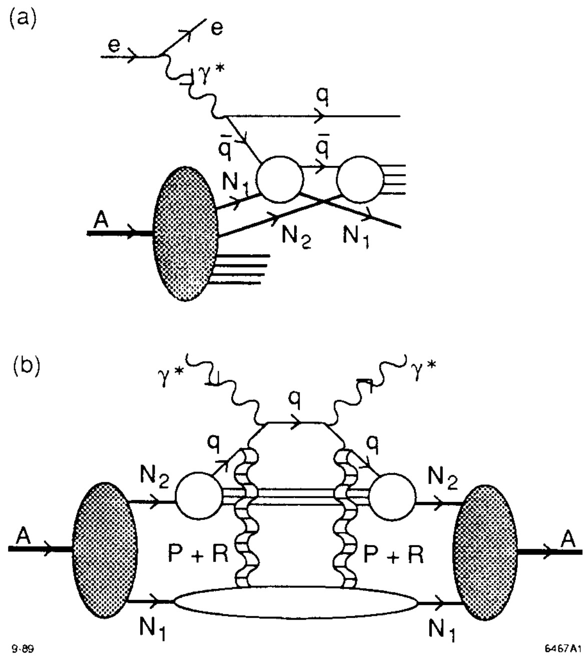

Figure 10. (a) The double–scattering amplitude that shadows the direct interaction of the anti–quark with N_2.
(b) The same mechanism as in (a), drawn in the traditional "hand–bag" form. Pomeron and Reggeon exchange between the quark line and N_1 are explicitly illustrated.

The predictions for the effective number of nucleons $A_{eff}(x)/A$ are shown in Fig. 11 for A = 12, 64, and 238. One observes shadowing below x $\simeq$ 0.1 and an anti-shadowing peak around x $\simeq$ 0.15. The shadowing effects are roughly logarithmic on the mass number A. The magnitude of shadowing predicted by the model is consistent with the data for x > 0.01; below this region, one expects higher-twist and vector-meson dominance shadowing to contribute. For x > 0.2 other nuclear effects must be taken into account. Most of the parameters used in the model are assigned typical hadronic values. The critical quantity is the effective quark-nucleon cross section σ which controls the magnitude of shadowing effect near x = 0: a larger value of σ implies a larger $\overline{q}^* N$ cross section and thus more shadowing. Notice that σ is the effective cross section at zero $\overline{q}$ virtuality, thus the typical value (a) entering the calculation is somewhat smaller. The magnitude of anti-shadowing is determined the real-to-imaginary-part ratio of the Reggeon scattering amplitude.

Our semi-quantitative analysis shows that parton multiple-scattering process provides a mechanism for explaining the observed shadowing at low x in the EMC–SLAC data. The existence of anti-shadowing requires the presence of regions

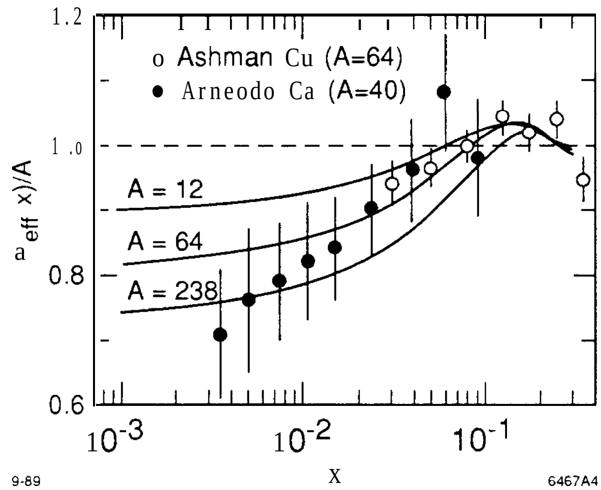

Figure 11. The predicted ratio of $A_{eff}(x)/A$ of the multi–scattering model in the low x region for different nuclear mass number. The data points are results from the EMC experiment for Cu and Ca.

where the real part of the $\overline{q}$ – N amplitude dominates over the imaginary part. The constructive interference which gives anti-shadowing in the x $\sim$ 0.15 region is due in this model to the phase of the Reggeon α = $1/2$ term. The phase follows from analyticity and is dictated by the shape of the structure functions at low x. We could utilize additional terms (at lower values of α) to parameterize other bound-state contributions which vanish as higher powers of x, but in practice their qualitative effect would be indistinguishable from the our simplified model. These results show that for reasonable values of the quark- and anti-quark-nucleon cross section, one can understand the magnitude of the shadowing effect at small x. Moreover, if one introduces an $\alpha_R \simeq 1/2$ Reggeon contribution to the $\overline{q}N$ and qN amplitudes, the real phase introduced by such a contribution automatically leads to "anti-shadowing" (effective number of nucleons $F_2^A(x, Q^2)/F_2^N(x, Q^2)$ > A) at x $\simeq$ 0.15 of the few percent magnitude seen by the SLAC and EMC experiments.[72,73] The analysis also provides the input or starting point for the log Q^2 evolution of the deep inelastic structure functions, as given for example by Mueller and Qiu.[81] The parameters for the effective q-nucleon cross section required to understand shadowing phenomena provide important information on the interactions of quarks in nuclear matter.

The analysis presented here correlates shadowing phenomena to microscopic quark-nucleon parameters. This approach also provides a dynamical and analytic explanation of anti-shadowing, confirming the conjecture of Nikolaev and Zakharov[82] who predicted that such an effect must exist on the basis of conservation laws. Using the perturbative QCD factorization theorem for inclusive reactions, the same analysis can be extended to Drell-Yan and other fusion processes, taking into account the separate dependence on the valence and sea quarks. Thus some shadowing and anti-shadowing should also be observable in the nuclear structure function $F_2^A(x_2, Q^2)$ extracted from massive lepton pair production on nuclear targets at low x_2. However, unlike pion excess models, the non-additive nuclear effect is not restricted to sea quarks.

This microscopic approach to shadowing and anti-shadowing analysis also has implications of the nature of particle production for virtual photoabsorption in nuclei. At high Q^2 and x > 0.3, hadron production should be uniform throughout the nucleus. At low x where shadowing occurs, the inelastic reaction occurs mainly at the front surface. These features can be examined in detail by studying non-additive multi-particle correlations in both the target and current fragmentation region. The same types of multi-scattering "fan" diagrams also appear in the analysis of the saturation of the gluon distribution at small x.[83]

7. CONCLUSIONS

In these lectures I have emphasized some of the remarkable features and complexities of the hadron and nuclear wave functions in QCD. By far, the simplest description of the hadron is given in terms of the light-cone Fock expansion, which provides a consistent covariant representation of the hadron wave function in terms of current quarks and gluons. This basis also allows a discrete computer simulation of the complete quantum field theory which faithfully reflects renormalizability and other properties of the continuum theory.

Nevertheless, the hadron wave-function must contains a large number of degrees of freedom in the light-cone basis. Part of the complexity is due to the lack of understanding of the QCD vacuum; it is now clear that the zero modes of the gauge field theory carry topological quantum numbers of the theory. The other complexities of the Fock basis have to do with the nature of confinement and the QCD couplings. The simulation of asymptotic freedom and chiral symmetry effects evidently require higher Fock states with multiple gluon and quark-pair components. The hardness of the QCD amplitudes implies that far-off shell fluctuations of the hadron wave function are present with a probability that only decreases as an inverse power of the virtuality. This implies relatively large probabilities for heavy flavor fluctuations, massive pair fluctuations, and high momentum components, much higher than the exponentially suppressed probabilities expected in a soft theory. The concept of "intrinsic hardness"' of the multi-particle amplitudes in hadron and nuclear wave functions leads to an understanding of a many diverse phenomena, such the observation of charm and charmonium at large longitudinal momentum and high-momentum "cumulative" effects in nuclear target experiments. The relatively large cross section for charm production at threshold predicted by intrinsic charm also provides an unexpected explanation for the spin correlation anomaly in elastic proton scattering and an explanation of the decrease of color transparency in quasi-elastic pp scattering at the same energy. The strong effects of coalescence particle interactions at low relative velocity also leads to an understanding of J/ψ suppression in heavy ion collisions and the prediction of nuclear bound-quarkonium.

There a number of important ways in which experiment can resolve and probe fundamental structure, particularly in electroproduction experiments where one can look at the entire final state. The traditional focus of electroproduction experiments has been tests of perturbative QCD predictions for the logarithmic evolution of deep inelastic structure functions due to gluonic radiation from the struck quark. This logarithmic effect is independent of the detailed structure of the proton itself. Tests of the leading twist PQCD evolution have been largely successful; however, at moderate values of momentum transfer there remains important questions and ambiguities concerning the magnitude and origin of higher twist corrections, the behavior of $R = \sigma_L/\sigma_T$, the origin of quark spin correlations, the shape of heavy sea components, and the gluon distribution. The non-singlet Regge behavior of structure functions has not been checked to high precision.

The interest in electroproduction has now turned to the basic problem of understanding the structure of the proton in terms of its quark and gluon degrees of freedom. Elastic and inelastic lepton scattering is still the best "microscope" for probing the fundamental structure of the nucleon. One is interested in testing the implications of non-perturbative QCD for the "intrinsic" multi-particle coherent bound-state structure of the nucleon. Information on the distribution amplitude $\phi_N(x_1, x_2, x_3, Q)$, the covariant wave function describing the correlations of valence quarks in the nucleon bound-state, can be obtained from measurements of form factors and other exclusive channels. Information on the complete multi-particle quark and gluon degrees of freedom requires detailed coincidence measurements of the final state hadrons, especially the target region. Nuclear targets play a valuable role in these measurements by modifying the hadronization and dynamics of the recoil quark jet over distances measured in fermi's, and by filtering out various components of the hadron wave function.

The following are just a few of the ways electroproduction experiments can probe basic QCD phenomena:

- Formation zone physics: study the quantum coherence and the time scales controlling the hadronization of quark jets propagating through a nucleus.

- Collision broadening: study the final state elastic interactions of the recoil quark jet as it propagates through a nuclear target.
- Anomalous spin correlations: study the spin structure functions and helicity effects in the final state, including correlations with strange particles.
- Intrinsic Charm: confirm the anomalous components of the charm structure functions of the proton seen at large x_{Bj}. Study charmonium and open charm production in the target fragmentation region.
- Color Transparency and Color Filter: study nuclear dependence of quasi-elastic reactions to separate short-range perturbative versus long-range non-perturbative phenomena. Remarkably, the cross section for large momentum transfer quasi-elastic scattering such as $ep \rightarrow ep$ in a nucleus is predicted in PQCD to be free of final state absorption corrections since the scattering is dominated by fluctuations of the valence-quark wave-functions with small transverse size.
- Photo-and electroproduction of charmonium states: provide constraints on the gluon distribution of the proton in the photon-gluon fusion model; use the nuclear dependence to test gluon shadowing and determine the ψN cross section as a measure of the basic size of quarkonium systems.
- Exclusive charm channels, e.g. $\gamma^* p \rightarrow \overline{D}\Lambda_c$: tests predictions of relatively large cross sections for the production of charm baryons near threshold as well as predictions for high momentum intrinsic charm components in the proton wave function.
- Nuclear-bound quarkonium: study electroproduction just below the threshold in $\gamma^* A \rightarrow \eta_c A$ reactions to identify nuclear-bound charmonium states such as $\eta_c^3 He$, novel bound states predicted to exist due to the attractive QCD van der Waals gluonic exchange potential.
- Quark-diquark structure of the proton: study correlations of final state hadrons in the target fragmentation region.
- Exclusive nuclear amplitudes such as $\gamma^* d \rightarrow np$: test PQCD "reduced amplitude" predictions.
- Prompt photon emission: study anomalous soft-photon production as a clue to hadronization mechanisms.
- Diffractive electroproduction such as $\gamma^* p \rightarrow \rho\, p$ on proton or nuclear targets: probe Pomeron coupling to systems of variable size and measure multi-gluon exchange form factors.
- Diffractive π and η photoproduction: identify and probe the QCD "Odderon" (odd C contribution to high energy scattering from three gluon exchange,

etc.) and its coupling.

- Exclusive channels, such as $ep \to eN^*$ at large Q^2: measure the fundamental distribution amplitudes (valence wave functions) of the proton and baryonic resonances; extend meson form factor measurements; test PQCD scaling laws for $\gamma^* p \to MN$ reactions.
- Exclusive Compton scattering at high momentum transfer $\gamma^* p \to \gamma p$: check perturbative QCD predictions.
- Exclusive Compton scattering on nuclei such as $\gamma^* D \to \gamma D$: search for "hidden color" multi-quark resonances predicted by QCD.
- Electron-positron asymmetry in $e^{\pm} p \to e^{\pm} \gamma X$: test fractional charges of quarks; measure new type of valence structure function.
- Cumulative Effect in $\gamma^* A \to HX$: measure the production of fast hadrons in the backward direction well beyond the kinematic limit for a proton target can identify anomalous short-range correlations predicted by PQCD.
- Intrinsic hardness: test PQCD predictions for high transverse momentum pair correlations in proton and nuclear intrinsic momentum wave functions.
- Spin-one structure functions for electroproduction on deuteron target: test PQCD predictions for high spin structure functions requiring multi-quark coherence.
- Shadowing and anti-shadowing: study deviations from uniform nuclear linear A-dependence behavior in inclusive and exclusive channels due to quark–nucleon scattering and long-range coherence.

ACKNOWLEDGEMENTS

Some of the material presented here is based on collaborations with others, particularly G. de Teramond, P. Hoyer, G. P. Lepage, H. J. Lu, A. H. Mueller, and I. Schmidt. I wish to thank Professor A. Zichichi and his staff for their outstanding hospitality and for providing such a stimulating atmosphere for physics at Erice. I also wish to thank my scientific secretaries, Boris Kastening, and Stephen Titard for their assistance in preparing the discussion session. Part of these lectures were also presented at the conference QCD90.

REFERENCES

1. For further background and references to these topics see S. J. Brodsky and G. P. Lepage, in *Quantum Chromodynamics*, edited by A. H. Mueller, (World Scientific, 1990), and S. J. Brodsky, lectures given at *The 27th International School* of *Subnuclear Physics: The Challenging Questions,* Erice, Italy, 1989.
2. S. J. Brodsky and P. Hoyer, to be published.
3. G. Bertsch, S. J. Brodsky, A. S. Goldhaber, and J. Gunion, Phys. Rev. Lett. 47, 297 (1981).
4. J. P. Ralston and B. Pire, Phys. Rev. Lett. 61, 1823 (1988), University of Kansas preprint 90–0548 (1990).
5. A. H. Mueller, *Proc. XVII Recontre de Moriond* (1982); S. J. Brodsky, *Proc. XIII International Symposium on M&particle Dynamics,* Volendam (1982); S. J. Brodsky and A. H. Mueller, Phys. Lett. 206B, 685 (1988). and references therein.
6. S. J. Brodsky and G. de Teramond, Phys. Rev. Lett. 60, 1924 (1988).
7. See S. J. Brodsky and A. H. Mueller, Ref. 5.
8. S. J. Brodsky and H. J. Lu, Phys. Rev. Lett. 64, 1342 (1990).
9. S. J. Brodsky and I. A. Schmidt, Phys. Lett. B234, 144 (1990).
10. For a review of the EMC spin crisis, see M. Karliner, 24th Rencontre de Moriond, Mar 1989; preprint TAUP 1730-89.
11. S. J. Brodsky and I. A. Schmidt, SLAC-PUB-5169, 1990, to be published in Phys. Rev. D.
12. T. Heinzl, S. Krusche, E. Werner, Regensburg University preprint TPR–90–44 (1990).
13. H. C. Pauli and S. J. Brodsky, Phys. Rev. D32, 1993, 2001 (1985); T. Eller, H. C. Pauli and S. J. Brodsky, Phys. Rev. D35, 1493, (1987). A detailed report on the development of DLCQ for gauge theories is in preparation.
14. K. Hornbostel, S. J. Brodsky, and H.-C. Pauli, Phys. Rev. D41, 3814 (1990); K. Hornbostel, SLAC-0333, Ph. D. thesis, unpublished (1988); and M. Burkardt, Nucl. Phys. A504, 762 (1989); and references therein.
15. A. Tang, S. Brodsky, H. C. Pauli, and M. Krautgartner, to be published.
16. Exclusive processes in QCD are reviewed in S. J. Brodsky and G. P. Lepage, Ref. 1.)

17. By definition, quasi-elastic processes are nearly coplanar, integrated over the Fermi motion of the protons in the nucleus. Such processes are nearly exclusive in the sense that no extra hadrons are allowed in the final state.

18. A. S. Carroll, et al., Phys. Rev. Lett. 61, 1698 (1988).

19. B. K. Jennings and G. A. Miller, Phys. Lett. B236, 209 (1990). and University of Washington preprint (1990).

20. G. R. Farrar, H. Liu, L. L. Frankfurt, M. I. Strikman, Phys. Rev. Lett. 61, 686 (1988).

-2-l: For additional discussion, see also, A. B. Kaidalov, presented at the LEAR Workshop (1990).

22. G. R. Court, et al., Phys. Rev. Lett. 57, 507 (1986).

23. For an alternative explanation, see Ref. 4.

24. S. J. Brodsky and P. Hoyer, Phys. Rev. Lett. 63, 1566 (1990); S. J. Brodsky, C. Peterson. and N. Sakai, Phys. Rev. D23, 2745 (1981). E. Hoffmann and R. Moore, Z. Phys. C20, 91 (1990). For a recent estimate of intrinsic charm matrix elements from OZI-violation in baryons, see T. Hatsuda and T. Kunihiro, CERN-TH. 5386 (1990).

25. J. Badier, et al., Z. Phys. C20, 101 (1983); Phys. Lett. 104B, 335 (1981). P. Charpentier, Saclay Thesis CEA-N-237 (1984).

26. D. M. Alde, et al., Phys. Rev. Lett. 64, 2479 (1990), Los Alamos preprint LA-UR-90-2331 (1990), and references therein.

27. G. T. Bodwin, S. J. Brodsky, and G. P. Lepage, Phys. Rev. D39, 3287 (1989).

28. J. Napolitano et al., Phys. Rev. Lett. 61, 2530 (1988).

29. For a recent review on the status of di-baryon hidden color resonances, see E. Lomon, MIT preprint (1990).

30. S. J. Brodsky, G. de Teramond, and I. Schmidt, Phys. Rev. Lett. 64, 1011 (1990).

31. The signal for the production of almost-bound nucleon (or nuclear) charmonium systems near threshold is the isotropic production of the recoil nucleon (or nucleus) at large invariant mass $M_X \simeq M_{\eta_c}$.

32. V. N. Gribov and L. N. Lipatov, Sov. J. Nucl. Phys. 15, 438 and 675 (1972).

33. J. D. Bjorken, Phys. Rev. D1, 1376 (1970).

34. See, for example, S. J. Brodsky, J. Ellis, M. Karliner, Phys. Lett. B206, 309 (1988).

35. R. Blankenbecler, S. J. Brodsky Phys. Rev. D10, 2973 (1974); J. F. Gunion, Phys. Rev. D10, 242 (1974); S. J. Brodsky and J. F. Gunion, Phys. Rev. D19, 1005 (1979).

36. M. B. Einhorn and J. Soffer, Nucl. Phys. B274, 714 (1986).

37. S. J. Brodsky and G. P. Lepage, Phys. Rev. D22, 2157 (1980).

38. J.D. Bjorken, J. Kogut, D. Soper, Phys. Rev. D3, 1382 (1971).

39. Z. F. Ezawa, Nuovo Cim. 23A, 271 (1974).

40. G. P. Lepage, Proceedings, SLAC Summer Institute (1981).

41. S. J. Brodsky and G. P. Lepage, *Proc. of the Int. Symp. on High Energy Physics with Polarized Beams and Polarized Targets,* Lausanne, Switzerland (1980).

42. See, e. g., F. Martin, Phys. Rev. D19, 1382 (1979); M. Glück, E. Reya, and W. Vogelsang, Dortmund University preprint DO-TH-89/3 (1989).

43. P. Aurenche, *et al.*, Phys. Rev. D39, 3275 (1989).

44. Structure functions for meson, baryon, and nuclear bound states in QCD in one-space and one-time dimensions have been computed numerically by diagonalizing the light-cone Hamiltonian. See Ref. 14.

45. See Ref. 37.

46. F. E. Close, *An Introduction to Quarks and Partons*, Academic Press (1979).

47. J. Kuti and V. F. Weisskopf, Phys. Rev. D4, 3418 (1971).

48. The position α_R of J-plane singularities in the forward virtual Compton amplitude are Q^2–independent, and thus the non-singlet Reggeon behavior $F_2^{NS}(x, Q^2) \sim x^{1-\alpha_R}$ at $x \to 0$ must be unaffected by QCD evolution. We thank J. Collins for conversations on this point.

49. S. J. Brodsky, F. E. Close and J. F. Gunion, Phys. Rev. D5, 1384 (1972).

50. W. Weisberger, Phys. Rev. D5, 2600 (1972); S. J. Brodsky, F. E. Close and J. F. Gunion, Phys. Rev. D8, 3678 (1973); S. J. Brodsky and I. Schmidt, unpublished. This result assumes that the valence quark mass only appears in the light-cone kinetic energy $\sum(k_\perp^2 + m^2)/x$.

51. One can identify the ultraviolet divergences at $x \to 0$ for sea quarks with the renormalization of the gluon propagator (which cancels in the proton–neutron mass difference.)

52. M. L. Goldberger and F. E. Low, Phys. Rev. 176, 1778 (1968); see also: T. Erber, Ann. Phys. 6, 319 (1959).

53. Strictly speaking, the bound-valence structure function of the proton refers to a proton in the extended QCD which contains chargeless quark pairs. Since these quarks are spectators in the deep inelastic lepton-proton cross sections, this should be a minor effect.

54. For discussion and references see M. Damashek and F. J. Gilman, Phys. Rev. D1, 319 (1970).

55. We neglect here the $\mathcal{O}(e^6)$ light-by-light scattering contributions to the forward Compton amplitude.

56. To leading order in α we can ignore higher order processes in the total cross section such as Compton scattering.

57. We neglect processes higher order in α_{QED} such as pair production in the electromagnetic field of the quark d.

58. For a derivation of the Reggeon contribution to the leading twist structure functions, see P. V. Landshoff, J. C. Polkinghorne and R. Short, Nucl. Phys. B28, 224 (1971), and S. J. Brodsky, F. E. Close, and J. F. Gunion, Ref. 50.

59. As usual we neglect hadronization effects and other final-state interactions at high energies.

60. A. Kernan, G. VanDalen Phys. Rep. 106, 207 (1984); S. P. K. Tavernier, Rep. Prog. Phys. 50, 1439 (1987); U. Gasparini, *Proc. XXIV Int. Conf. on High Energy Physics*, (R. Kotthaus and J. H. Kühn, Eds., Springer 1989), p. 971.

61. Detailed predictions for the contribution of intrinsic charm to the nucleon charmed quark structure functions and comparisons with existing lepto-production data are given by E. Hoffmann and R. Moore, Ref. 24.

62. M. MacDermott and S. Reucroft, Phys. Lett. 184B, 108 (1987).

63. S. F. Biagi, *et al.*, Z. Phys. C28, 175 (1985). See also P. Coteus, *et al.*. Phys. Rev. Lett. 59, 5030 (1987).

64. S. J. Brodsky, P. Hoyer, C. Peterson, and N. Sakai, Phys. Lett. 93B, 451 (1980); S. J. Brodsky, C. Peterson, and N. Sakai, Ref. 24.

65. S. J. Brodsky, J. F. Gunion, and D. E. Soper, Phys. Rev. D36, 2710 (1987).

66. K. J. Anderson, *et al.*, Phys. Rev. Lett. 42, 944 (1979); A. S. Ito, *et al.*, Phys. Rev. D23, 604 (1981); P. Bordalo, *et al.*, Phys. Lett. 193B, 368 (1987).

67. Yu. M. Antipov, *et al.*, Phys. Lett. 76B, 235 (1978); M. J. Corden, *et al.*, Phys. Lett. 110B, 415 (1982); J. Badier, *et al.*, Ref. 25; S. Katsanevas, *et al.*, Phys. Rev. Lett. 60, 2121 (1988).

68. P. Hoyer, M. Vanttinen, and U. Sukhatme, HU-TFT-90-14, (1990.)

69. S. J. Brodsky and P. Hoyer, Ref. 24.

70. Alternatively, the individual charmed quarks can fragment into final state charmed hadrons either by hadronization or by coalescing with co-moving light quark spectators from the beam. This effect can explain the depletion of the ratio of J/ψ to continuum muon pairs in high transverse energy nucleus-nucleus collisions. See S J. Brodsky and A. H. Mueller, Ref 5.

71. S. J. Brodsky, H. E. Haber, and J. F. Gunion, in *Anti-pp Options for the Supercollider,* Division of Particles and Fields Workshop, Chicago, IL, 1984, edited by J. E. Pilcher and A. R. White (SSC-ANL Report No. 84/01/13, Argonne, IL, 1984), p. 100. S. J. Brodsky, J. C. Collins, S. D. Ellis, J. F. Gunion, and A. H. Mueller, published in Snowmass Summer Study 1984, p. 227.

72. J. Ashman *et al.*, Phys. Lett. 202B, 603 (1988) and CERN-EP/88-06 (1988) M. Arneodo *et al.*, Phys. Lett. 211B, 493 (1988)

73. R. G. Arnold *et al.*Phys. Rev. Lett. 52, 727 (1984) and SLAC-PUB-3257 (1983)

74. J. S. Bell, Phys. Rev. Lett. 13, 57 (1964)

75. L. Stodolsky, Phys. Rev. Lett. 18, 135 (1967)

76. S. J. Brodsky and J. Pumplin, Phys. Rev. 182, 1794 (1969)

77. J. J. Sakurai and D. Schildknecht, Phys. Lett. 40B, 121 (1972); Phys. Lett. 41B, 489 (1972); Phys. Lett. 42B, 216 (1972)

78. R. J. Glauber, in *Lectures in Theoretical Physics,* edited by W. E. Brittin *et al.* (Interscience, New York, 1959), vol. I

79. T. H. Bauer, R. D. Spital, D. R. Yennie and F. M. Pipkin, Rev. Mod. Phys. 50, 261 (1978)

80. P. V. Landshoff, J. C. Polkinghorne and R. D. Short, Nucl. Phys. B28, 225 (1971)

81. A. H. Mueller and J. Qiu, Nucl. Phys. B268, 427 (1986) J. Qiu, Nucl. Phys. B291, 746 (1987)

82. N.N. Nikolaev and V. I. Zakharov, MPI-PAE-PTh-11/90, (1990); Physics Letters 55B, 397 (1975); Sov. J. Nucl. Phys. 21, 227 (1975).

83. A.H. Mueller, CU-TP-475, DESY Lectures given at the Small-x Workshop, DESY, May (1990).